



저작자표시-비영리-변경금지 2.0 대한민국

이용자는 아래의 조건을 따르는 경우에 한하여 자유롭게

- 이 저작물을 복제, 배포, 전송, 전시, 공연 및 방송할 수 있습니다.

다음과 같은 조건을 따라야 합니다:



저작자표시. 귀하는 원저작자를 표시하여야 합니다.



비영리. 귀하는 이 저작물을 영리 목적으로 이용할 수 없습니다.



변경금지. 귀하는 이 저작물을 개작, 변형 또는 가공할 수 없습니다.

- 귀하는, 이 저작물의 재이용이나 배포의 경우, 이 저작물에 적용된 이용허락조건을 명확하게 나타내어야 합니다.
- 저작권자로부터 별도의 허가를 받으면 이러한 조건들은 적용되지 않습니다.

저작권법에 따른 이용자의 권리는 위의 내용에 의하여 영향을 받지 않습니다.

이것은 [이용허락규약\(Legal Code\)](#)을 이해하기 쉽게 요약한 것입니다.

[Disclaimer](#)

**A THESIS  
FOR THE DEGREE OF MASTER OF SCIENCE**

**Anti-inflammatory and anti-osteoporotic effects of  
2,4'-dihydroxybenzophenone**

**MIRISSA HEWAGE DUMINDU KAVINDA**

Department of Marine Life Sciences

SCHOOL OF BIOMEDICAL SCIENCE

JEJU NATIONAL UNIVERSITY

REPUBLIC OF KOREA

February 2023

**Anti-inflammatory and anti-osteoporotic effects of 2,4'-dihydroxybenzophenone**

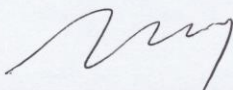
**Mirissa Hewage Dumindu Kavinda**

**(Supervised by Professor Gi-Young Kim)**

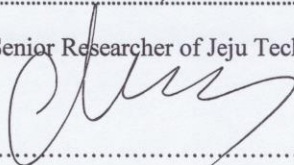
A thesis submitted in partial fulfillment of the requirement for the degree of masters

February 2023

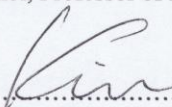
The thesis has been examined and approved by



.....  
Sanghyuck Kang, Senior Researcher of Jeju Techno Park



.....  
Yung Hyun Choi, Professor of Dong-Eui University



.....  
Gi-Young Kim, Professor of Jeju National University

February 2023

.....  
Date

Department of Marine Life Science  
GRADUATE SCHOOL  
JEJU NATIONAL UNIVERSITY

## **Acknowledgments**

First and foremost, I would like to express my sincere gratitude to my academic supervisor, Professor Kim-Gi-Young for guiding and encouraging me throughout my master's degree program. His valuable ideas and continuous encouragement throughout my master's degree program immensely helped me to successfully complete my master's degree.

Then, I would like to thank my lab members, especially Dr. Neelaka Molagoda, Mr. Hasitha Karunaratne, Mr. Chanaka Jayasinghe, Mr. Gihan Kavinda Athapaththu, Mr. Senel Sanjaya and Mr. An Do Won for their continuous encouragement, valuable comments, and help throughout this challenging period. I also express my gratitude to my wife Oshini Nimesha Prathibani who helped me immensely throughout this challenging period.

However, I am the only person responsible for any error in the thesis and all the comments on this are highly appreciated.

## Table of Contents

<b>Acknowledgments</b> .....	ii
<b>List of Tables</b> .....	v
<b>List of Figures</b> .....	vi
<b>Chapter 01</b> .....	vii
<b>Abstract</b> .....	1
<b>1. Introduction</b> .....	2
<b>2. Materials and methods</b> .....	5
2.1. <i>Reagents and antibodies</i> .....	5
2.2. <i>Cell culture and cell viability assay</i> .....	5
2.3. <i>Analysis of viable cell count and dead cell population</i> .....	6
2.4. <i>NO assay</i> .....	6
2.5. <i>Isolation of total RNA from RAW 264.7 macrophages and reverse transcription polymerase chain reaction (RT-PCR)</i> .....	6
2.6. <i>Measurement of IL-12 and TNF-<math>\alpha</math> cytokine levels</i> .....	8
2.7. <i>Molecular interaction between TLR4/MD2 receptor complex and DHP</i> .....	8
2.8. <i>Protein extraction and western blotting</i> .....	8
2.9. <i>Immunofluorescence staining</i> .....	9
2.10. <i>Maintenance of zebrafish embryo and larvae</i> .....	9
2.11. <i>Evaluation of heart rate, abnormality, and mortality in LPS-microinjected zebrafish larvae</i> .....	10
2.12. <i>Neutral red and sudan black staining</i> .....	10
2.13. <i>Isolation of total mRNA from zebrafish larvae and RT-PCR</i> .....	11
2.14. <i>Detection of mtROS in RAW 264.7 cells and zebrafish larvae</i> .....	11
2.15. <i>Measurement of mitochondrial membrane depolarization</i> .....	11
2.16. <i>Statistical analysis</i> .....	12
<b>3. Results</b> .....	13
3.1. <i>DHP decreases mortality and abnormality, and recovered the heart rate in LPS-microinjected zebrafish larvae</i> .....	13
3.2. <i>DHP inhibits LPS-induced proinflammatory mediators in zebrafish larvae and decreases recruitment of macrophages and neutrophils to the infected sites</i> .....	17
3.3. <i>High concentrations of DHP moderately decreases viability of RAW 264.7 macrophages</i> ...	20
3.4. <i>DHP inhibits LPS-induced proinflammatory mediators in RAW 264.7 macrophages</i> .....	23
3.5. <i>DHP potentially binds to TLR4/MD2 receptor complex</i> .....	25
3.6. <i>DHP inhibits the MyD88-IRAK4-NF-<math>\kappa</math>B signaling pathway</i> .....	28
3.7. <i>DHP decreases LPS-induced mitochondrial membrane depolarization and mtROS production in RAW 264.7 macrophages</i> .....	31

3.8. DHP decreases LPS-induced mtROS production in zebrafish larvae .....	34
3.9. DHP potently binds with TLR4 and alleviate mitochondrial depolarization in RAW 264.7 macrophages.....	36
<b>4. Discussion</b> .....	<b>38</b>
<b>5. References</b> .....	<b>41</b>
<b>Appendix</b> .....	<b>48</b>
<b>Chapter 02</b> .....	<b>56</b>
<b>1. Introduction</b> .....	<b>58</b>
<b>2. Materials and methods</b> .....	<b>61</b>
2.1. Regents and antibodies .....	61
2.2. Cell culture and MTT assay.....	61
2.3. Flow cytometry analysis .....	62
2.4. Alkaline phosphatase (ALP) and alizarin red staining.....	62
2.5. Isolation of mRNA from MC3T3-E1 cells and reverse transcription-polymerase chain reaction (RT-PCR).....	62
2.6. Western blotting.....	63
2.7. Zebrafish maintenance .....	64
2.8. Vertebral formation in zebrafish larvae .....	64
2.9. Isolation of mRNA from zebrafish larvae and RT-PCR.....	65
2.10. Statistical analysis .....	65
<b>3. Results</b> .....	<b>66</b>
3.1. DHP at a concentration of 100 $\mu$ M is cytotoxic to MC3T3-E1 preosteoblast cells .....	66
3.2. DHP promotes osteoblast differentiation in MC3T3-E1 preosteoblast cells .....	69
3.3. DHP enhances vertebral formation in zebrafish larvae .....	72
3.4. DHP upregulates GSK-3 $\beta$ phosphorylation and subsequent $\beta$ -catenin activation .....	75
3.5. DHP abates PDS-induced anti-osteogenic properties in MC3T3E-1 cells .....	77
3.6. DHP alleviates PDS-induced osteoporosis in zebrafish larvae .....	80
<b>4. Discussion</b> .....	<b>83</b>
<b>5. References</b> .....	<b>86</b>

## List of Tables

Table 1: Primers used in this study for RT-PCR.....	7
Table 2 : Effects of DHP on mortality and abnormality in LPS-microinjected zebrafish .....	14
Table 3: Primer sequences used in this study.....	63

## List of Figures

<b>Fig. 1.1.</b> Structure of 2,4'-dihydroxybezophenone (DHP). .....	14
<b>Fig. 1.2.</b> DHP decreases mortality and abnormality in LPS-microinjected zebrafish larvae and recovers impaired heart rates.....	15
<b>Fig. 1.3.</b> DHP inhibits LPS-induced inflammatory responses in zebrafish larvae.....	18
<b>Fig. 1.4.</b> A high concentration of DHP slightly gives damage in RAW 264.7 macrophages..	21
<b>Fig. 1.5.</b> DHP inhibits proinflammatory mediators in LPS-treated RAW 264.7 macrophages	24
<b>Fig. 1.6.</b> DHP possibly binds to mouse TLR4/MD2 receptor complex (3VQ1).. .....	26
<b>Fig. 1.7.</b> DHP possibly binds to human TLR4/MD2 receptor complex (3FXI). .....	27
<b>Fig. 1.8.</b> DHP inhibits TLR4 expression and the MyD88-IRAK4-NF- $\kappa$ B signaling pathway	29
<b>Fig. 1.9.</b> DHP inhibits LPS-induced mitochondrial membrane potential depolarization and mtROS production.....	33
<b>Fig. 1.10.</b> DHP decreases mtROS production and restores the heart rate in LPS-microinjected zebrafish larvae.....	35
<b>Fig. 1.11.</b> Inhibition of TLR4 signaling reduces LPS-induced mitochondrial membrane potential depolarization .....	36
<b>Fig. 2.1.</b> DHP at a concentration of 100 $\mu$ M decreases viability of MC3T3-E1 preosteoblasts.. .....	67
<b>Fig. 2.2.</b> DHP stimulates osteoblast differentiation .....	70
<b>Fig. 2.3.</b> DHP promotes vertebral formation in zebrafish larvae. ....	73
<b>Fig. 2.4.</b> DHP promotes GSK-3 $\beta$ phosphorylation at SER9 and subsequent $\beta$ -catenin activation. ....	76
<b>Fig. 2.5.</b> DHP restored osteoblast differentiation impaired by prednisolone (PDS).....	78
<b>Fig. 2.6.</b> DHP recovers prednisolone (PDS)-induced impaired vertebral formation.....	81



## **Chapter 01**

# **2,4'-Dihydroxybenzophenone alleviates LPS-induced endotoxic shock by inhibiting the TLR4/MD2 signaling pathway**

## Abstract

2,4'-Dihydroxybenzophenone (DHP) is derived from the herbs of *Garcinia xanthochymus*; no biochemical properties have been elucidated. In this study, we investigated whether DHP alleviates LPS-induced inflammatory responses and endotoxin shock in RAW 264.7 macrophages and zebrafish larvae. In LPS-microinjected zebrafish larvae as an endotoxin shock model, DHP dramatically attenuates mortality and morphological abnormality and restored reduced heart rate. Moreover, the expression of proinflammatory mediators, including nitric oxide, tumor necrosis factor- $\alpha$  (TNF- $\alpha$ ), and interleukin-12 (IL-12), was dramatically reduced in the presence of DHP accompanied by mitigation of macrophage and neutrophil recruitment to the inflammatory sites. We revealed that DHP inhibits LPS-induced inflammatory response by downregulating pro-inflammatory mediators in RAW 264.7 macrophages. Molecular docking data predicted that DHP possibly binds to hydrophobic pocket of myeloid differentiation factor 2 (MD2) and occlude dimerization of Toll-like receptor 4 (TLR4) and MD2. Hence, DHP downregulated the TLR4-mediated intracellular signaling pathway, decreasing the expressions of myeloid differentiation primary response 88 (MyD88), phosphorylation of IL-1 receptor-associated protein kinase-4 (p-IRAK4), and nuclear factor- $\kappa$ B (NF- $\kappa$ B) in LPS-induced RAW 264.7 macrophages. Furthermore, we revealed that DHP inhibits mitochondrial reactive oxygen species (mtROS) during LPS-induced inflammatory conditions in RAW 264.7 macrophages and zebrafish larvae accompanied by the stabilization of mitochondrial membrane potential. Altogether, our study confirmed that DHP alleviates LPS-induced inflammation and endotoxin shock in vitro and in vivo by binding to TLR4/MD2 receptor complex and subsequently reducing mtROS production.

*Key words:* DHP, endotoxic shock, TLR4/MD2, mtROS

## 1. Introduction

Sepsis is a fatally life-threatening condition caused by an unbalanced immunological response to an infection, which is defined as organ failure and cardiovascular dysfunction, causing a significant increase of mortality rate of above 40% [1]. The most frequent sepsis is endotoxin shock driven by gram-negative bacterial infection, resulting in severely systemic inflammatory responses and low blood pressure [2]. Bacterial endotoxin (lipopolysaccharide, LPS), a cell wall component of gram-negative bacteria, is known to be a major cause of endotoxin shock, and excessive influx of LPS into the blood stream increases the mortality rate through the systemic inflammatory responses [3]. In particular, monomeric LPS is detected by serum LPS-binding protein (LBP), which transfers monomeric LPS to soluble or membrane-bound CD14, resulting in the release of LPS-bound CD14 from LBP by electrostatic repulsion [4, 5]. The LPS-bound CD14 is delivered to Toll-like receptor 4 (TLR4)/myeloid differentiation factor 2 (MD2) membrane receptor complex and subsequently promotes homodimerization of the receptor complex [4, 5]. Binding of monomeric LPS to TLR4/MD2 receptor complex triggers its conformational change and consequently leads to dimerization of the cytoplasmic toll-interleukin (IL)-1 (TIR) domain, which in turn recruits myeloid differentiation primary response 88 (MyD88) and IL-1 receptor-associated kinase (IRAK)-4 [6]. IRAK4 ultimately leads to the activation of nuclear transcription factor- $\kappa$ B (NF- $\kappa$ B), which transactivates expression of proinflammatory genes, such as inducible nitric oxide synthase (iNOS), IL-12, and tumor necrosis factor (TNF)- $\alpha$  [7]. LPS cause immune and nonimmune cells to produce a great deal of proinflammatory mediators including NO, IL-12, and TNF- $\alpha$ , which results in inflammatory tissue damages, low blood pressure, and multiple organ failure [1, 2]. Hence, many synthetic TLR4 antagonists and proteins have been identified to attenuate endotoxin shock [8, 9].

Mitochondria are well known for their function as energy producers in the cells and are

responsible for a variety of cellular processes such as cell cycle progression, cellular differentiation and growth, and inflammation [10]. Innate immune cells such as macrophages and neutrophils produce and employ mitochondrial reactive oxygen species (mtROS) as antimicrobial agents in host defense to eliminate invasive pathogens [11]. However, excessive mtROS production exerts mitochondrial damage and dysfunction, causing life-threatening organ damage such as sepsis [12, 13]. Cimolai et al. described that mitochondrial dysfunction is widely found in organ dysfunction in sepsis by increasing mtROS production, causing decreased O<sub>2</sub> consumption and mitochondrial membrane potential, and consequent energy depletion [14]. In this regard, Victor et al. reviewed that antioxidants targeting mtROS has a potential therapy against mtROS-mediated sepsis [15]. Additionally, Kong et al. reported that, in double knockout mice lacking Nrf2 (*Nrf2*<sup>-/-</sup>) inflammatory sepsis was greater than wild-type (*Nrf2*<sup>+/+</sup>), which was significantly ameliorated by depletion of NADPH oxidase-dependent ROS production [16]. The protective function of Nrf2 in sepsis was highlighted and antioxidant compounds that activate the Nrf2-HO-1 signaling pathway such as plant-derived flavonoids improve mouse survival by inhibiting severe inflammatory responses [17, 18]. The above studies and reviews show that LPS triggers endotoxin shock by binding to the TLR4/MD2 complex and subsequent its activation, and at the time, excessively produced ROS play an essential role in endotoxin shock. Therefore, antioxidants or Nrf2 agonists has been considered to reduce endotoxin shock-mediated organ damage and mortality.

Benzophenone is a sweet-smelling organic compound in many fruits, and its derivatives have been widely used in cosmetics because of its powerful protective effect against ultraviolet light [19]. However, some researchers reported that benzophenone sensitizes DNA damage [20] and a potential toxicity through hydroxyl radicals [21], causing environmental risks. Besides, some adverse effects were reported that maternal benzophenone exposure exacerbates hippocampus development in mice and a human brain organoid model during pregnancy [22].

In the contrary, a benzophenone derivative, 4-geranyloxy-2-hydroxy-6-isoprenyloxybenzophenone, showed the strong inhibition rate of NO production in LPS-stimulated RAW 264.7 macrophages [23]. Additionally, garcinol, a polyisoprenylated benzophenone derivative isolated from *Garcinia indica* attenuated inflammatory cytokines and oxidative stress in ischemia-reperfusion injury by inhibiting the TLR4-mediated NF- $\kappa$ B signaling pathway [24]. In addition, there are few literatures on other distinct biochemical functions in vitro and in vivo. Another derivative used in this study, 2,4'-dihydroxybenzophenone (DHP) is derived from the herb, *Garcinia xanthochymus*, which is used for the synthesis of pharmaceutical agents [25]. Due to the lack of literature on DHP, its antioxidant and anti-inflammatory properties are yet to be discovered.

In this study, we investigated whether DHP alleviates LPS-induced inflammation and endotoxin shock by inhibiting the binding of LPS to TLR4/MD2 receptor complex. Additionally, we investigated whether DHP inhibits mtROS production both in vitro and in vivo during LPS-induced inflammation and endotoxin shock.

## 2. Materials and methods

### 2.1. Reagents and antibodies

DHP (Fig. 1.1) was purchased from ChemFaces (606-12-2, Wuhan, Hubei, China). Dulbecco's Modified Eagle medium (DMEM), fetal bovine serum (FBS), and antibiotic mixture were obtained from WELGENE Inc. (Gyeongsan-si, Gyeongsangbuk-do, Republic of Korea). Lipopolysaccharides (LPS from *Escherichia coli* O55:B5), 3-(4,5-Dimethylthiazol-2-yl)-2,5-diphenyltetrazolium bromide (MTT), and TLR4-IN-C34 were purchased from Sigma-Aldrich (St. Louis, MO, USA). Antibodies against p50 (sc-8414), p65 (sc-8008),  $\beta$ -actin (sc-69879), nucleolin (sc-13057), MyD88 (sc-74532), and peroxidase labeled anti-mouse immunoglobulins were purchased from Santa Cruz Biotechnology (Dallas, Texas, USA). Phospho (p)-IRAK4 (PA5-102849) was purchased from Thermo Fisher Scientific (Waltham, MA, USA). Peroxidase labeled anti-rabbit antibody was purchased from Koma Biotechnology (Seoul, Republic of Korea). Anti-rabbit Alexa Fluor 488 secondary antibody was purchased from Abcam (Cambridge, MA, UK), and Dako faramount aqueous mounting media was purchased from Dako (Carpinteria, CA, USA). All other chemicals were purchased from Sigma-Aldrich (St. Louis, MO, USA).

### 2.2. Cell culture and cell viability assay

RAW 264.7 macrophages were obtained from the American Type Culture Collection (Manassas, VA, USA) and cultured in DMEM supplemented with 5% FBS and antibiotic mixture at 37°C with 5% CO<sub>2</sub> in a humidified incubator. Briefly, the cells were seeded at  $1 \times 10^5$  cells/mL in 24-well plates and treated with the indicated concentrations of DHP (0–50  $\mu$ M) for 2 h followed by treatment with LPS (500 ng/mL) for 24 h. MTT (0.5 mg/mL) was added to each well and incubated it for 4 h. Then, formazan was dissolved with dimethyl sulfoxide and absorbance was measured at 570 nm wavelength (BioTek Instruments, Inc., Winooski, VT,

USA). In a parallel experiment, cell morphology was observed and imaged using a phase-contrast microscopy (Macrotech, Goyang-si, Gyeonggi-do, Republic of Korea).

### *2.3. Analysis of viable cell count and dead cell population*

RAW 264.7 macrophages were seeded at a density of  $1 \times 10^5$  cells/ml in 6-well plates and treated with the indicated concentrations of DHP 2 h before treatment with LPS (500 ng/mL) for 24 h. Then, the cells were harvested and washed with ice-cold phosphate-buffered saline (PBS) and incubated with a Muse Cell Count and Viability Kit (Luminex, Austin, TX, USA) for 5 min. Viable cell count and dead cell population were measured by Muse Cell Cycler (Luminex).

### *2.4. NO assay*

RAW 264.7 macrophages were seeded at  $1 \times 10^5$  cells/mL into 24-well plates and treated with given concentrations of DHP (0-25  $\mu$ M). LPS (500 ng/mL) was treated to the cells 2 h after DHP treatment and incubated for 24 h. NO production was measured using the Griess reagent assay [26].

### *2.5. Isolation of total RNA from RAW 264.7 macrophages and reverse transcription polymerase chain reaction (RT-PCR)*

RAW 264.7 macrophages were seeded at  $1 \times 10^5$  cells/mL into 6-well plates and treated with given concentrations of DHP (0-25  $\mu$ M) for 2 h followed by treatment with LPS (500 ng/mL) for 6 h. Total RNA was isolated from RAW 264.7 macrophages using easy-BLUE total RNA Extraction Kit (iNtRON Biotechnology, Seongnam-si, Gyeonggi-do, Republic of Korea) according to the manufacturer's instructions. Then, RNA was reverse transcribed using Moloney Murine Leukemia Virus (MMLV) Reverse Transcriptase Kit (Bioneer, Daejeon-si, Republic of Korea). Synthetic cDNA was amplified using specific primers in specified conditions [27]. All primer sequences are shown in Table 1.

Table 1: Primers used in this study for RT-PCR

Species	Gene	Primer sequences (5'→3')	Size (bp)	Accession No.
Mouse	<i>iNOS</i>	F: 5'-CCTCCTCCACCCTACCAAGT-3' R: 5'-CACCCAAAGTGCTTCAGTCA-3'	199	NM 010927.4
	<i>TNF-α</i>	F: 5'-ATGAGCACAGAAAGCATGAT-3' R: 5'-TACAGGCTTGTCACCTCGAAT-3'	276	NM 013693.3
	<i>IL-12p35</i>	F: 5'- AAGACATCACACGGGACCAA -3' R: 5'- GAGGATACCACTTCCCAACAG -3'	319	NM 001159424.3
	<i>GADPH</i>	F: 5'-ACCACAGTCCATGCCATCAC-3' R: 5'-CACCACCCTGTTGCTGTAGC-3'	450	NM 001289726.2
Zebrafish	<i>iNOS</i>	F: 5'-GGAGATGCAAGGTCAGCTTC-3' R: 5'-GGCAAAGCTCAGTGA CTTC-3'	137	NM_001104937.1
	<i>TNF-α</i>	F: 5'-TAGAACAACCCAGCAAAC-3' R: 5'-ACCAGCGGTAAAGGCAAC-3'	149	NM_212859.2
	<i>IL-12p35</i>	F: 5'-TCTAACTTCAGCGCAGTGGA-3' R: 5'-TGCGGTGGTGTAGTGAGTG-3'	334	NM_001007107.2
	<i>β-actin</i>	F: 5'-CGAGCGTGGCTACAGCTTCA-3' R: 5'-GACCGTCAGGCAGCTCATAG-3'	155	NM 131031.2



## 2.6. Measurement of IL-12 and TNF- $\alpha$ cytokine levels

ELISA kits (PEPROTECH, Cranbury, NJ, USA) were used to quantify the levels of IL-12 and TNF- $\alpha$  according to manufacturer's instructions. Briefly, RAW 264.7 macrophages ( $1 \times 10^5$  cells/ml) were seeded into a 24-well plate and treated with the indicated concentrations of DHP (0–25  $\mu$ M) for 2 h prior to stimulation with LPS (500 ng/mL) for 24 h. Supernatants were collected from each treatment, and amount of extracellular secreted IL-12 and TNF- $\alpha$  was analyzed.

## 2.7. Molecular interaction between TLR4/MD2 receptor complex and DHP

Crystal structures of mouse TLR4/MD2-lipid IVa complex (PDB ID: 3VQ1) [28] and human TLR4/MD2-*E. coli* LPS Ra complex (PDB ID: 3FXI) [29] were obtained from RCSB protein database bank (PDB), and molecular docking simulation was performed after removing lipid IVa and *E. coli* LPS Ra. Chemical structure of DHP (CID 220295; canonical SMILES, C1=CC=C(C(=C1)C(=O)C2=CC=C(C=C2)O)O) was obtained from PubChem (<https://pubchem.ncbi.nlm.nih.gov>, National Center for Biotechnology Information, Bethesda, MD, USA), and its structure was minimized. Interaction between TLR4-MD2 (a monomer) and DHP was performed using SwissDock [30]. Additionally, another molecular docking was simulated using Mcule [31], and the interaction poses were visualized UCSF chimera [32]. The 2D docking data were finally constructed using Discovery Studio Visualizer (<https://www.discover.3ds.com/discovery-studio-visualizer-download>).

## 2.8. Protein extraction and western blotting

Protein extraction and western blotting were performed as previously described [27]. Briefly, RAW 264.7 macrophages were seeded at  $1 \times 10^5$  cells/mL in 6-well plates and treated with the indicated concentrations of DHP (0–25  $\mu$ M). LPS (500 ng/mL) were treated 20 min after DHP treatment for 2 h. Then, the cells were washed with PBS, and nuclear and cytosolic proteins were extracted using NE-PER Nuclear and Cytoplasmic Extraction Reagents (Pierce,

Rockford, IL, USA). Protein quantification was determined using Bio-Rad Protein Assay (Bio-Rad; Hercules, CA, USA). Equal amounts of proteins (30 µg) were separated by SDS-polyacrylamide gel electrophoresis and transferred onto the PVDF membrane (Thermo Fisher Scientific) and immunoblotted with indicated antibodies. Bound antibodies were detected using an enhanced chemiluminescence plus kit (Thermo Fisher Scientific). The images were captured using ImageQuant LAS 500 (GE Healthcare Bio-Sciences AB, Uppsala, Sweden). The expressional value of nuclear and cytosolic proteins was normalized to the intensity level of β-actin and nucleolin, respectively, using ImageJ (National Institute of Health, Bethesda, MD, USA, [www.imagej.net](http://www.imagej.net)).

### *2.9. Immunofluorescence staining*

Immunofluorescence staining was performed as previously described [33]. Briefly, RAW 264.7 macrophages were seeded at  $1 \times 10^5$  cells/ml on 3% gelatin-coated coverslips and treated with DHP (0–25 µM) for 2 h prior to exposure to LPS for 1 h. The cells were fixed with 4% paraformaldehyde for 10 min at room temperature and permeabilized with 0.1% Triton X-100 for 10 min at room temperature. Then, the cells were blocked with 10% donkey serum and incubated with p65 or TLR4 antibody (1:100 in 10% donkey serum) for 16 h at 4°C. After washing with ice-cold PBST, Alexa Fluor 488 secondary antibody was added and incubated for 2 h at room temperature. The cells were counterstained with DAPI (300 nM) for 10 min, and the coverslips were mounted onto glass slides with Dako faramount aqueous mounting media. Fluorescence images were captured by a CELENA S Digital Imaging System (LogosBiosystems, Anyang, Gyeonggido, Republic of Korea).

### *2.10. Maintenance of zebrafish embryo and larvae*

Zebrafish were raised according to the relevant regulations and guidelines given by the Animal Care and Use Committee of Jeju National University (Jeju Special Self-governing province, Republic of Korea; approval No: 2022-0069). Zebrafish were raised as previously

described [27, 33].

### *2.11. Evaluation of heart rate, abnormality, and mortality in LPS-microinjected zebrafish larvae*

LPS microinjection and cardiac toxicity evaluation were performed as previously described [27, 33]. Briefly, 3 dpf zebrafish larvae were anesthetized using 0.04% tricaine prior to microinjection with LPS (0.5 mg/mL, 2 nL in each larva). LPS was microinjected into the yolk sac using a Drummond NANOJECT III Injector (Drummond Scientific, Broomall, PA, USA). After injecting LPS, the larvae were immediately placed in embryo medium containing the indicated concentrations (0–25  $\mu$ M) of DHP. Dead larvae were removed within 0.5 h post-injection (hpi). Each group of larvae (n=20) was cultured at 28.5°C and observed the survival rate and phenotypic abnormalities at 48 hpi. Additionally, after 24 hpi, the heart rate was manually counted for 1 min. All mentioned parameters were observed using stereomicroscopy (Olympus, Tokyo, Japan).

### *2.12. Neutral red and sudan black staining*

Neutral red and Sudan black stains were performed as previously described [33, 34]. LPS (0.5 mg/mL, 2 nL in each larva) or PBS, in the presence or absence of DHP (0–25  $\mu$ M), were microinjected in the yolk of 3 dpf zebrafish larvae and the larvae were stained using neutral red (macrophages) and sudan black (neutrophils) solution for 18 hpi. For neutral red staining, the larvae were incubated in 2.5  $\mu$ g/mL neutral red solution containing 0.003% PTU at 28.5°C in the dark for 8 h. Macrophages were observed using stereomicroscopy (Olympus). For sudan black staining, the larvae were fixed with 4% methanol-free paraformaldehyde for 2 h at room temperature and rinsed three times with PBS. Then, the larvae were incubated in sudan black solution for 40 min, and neutrophils were observed using stereomicroscopy (Olympus).

### 2.13. Isolation of total mRNA from zebrafish larvae and RT-PCR

LPS (0.5 mg/mL, 2 nL in each larva) or PBS were microinjected in the yolk of 3 dpf zebrafish and raised in the indicated concentrations of DHP (0–25  $\mu$ M) for 18 hpi. Total RNA was extracted using easy-BLUE Total RNA Extraction Kit (iNtRON Biotechnology). The RNA was reverse transcribed using MMLV Reverse Transcriptase Kit (Bioneer) and synthetic cDNA was amplified using specific primers [27]. All the primer sequences used in this study were shown in Table 1.

### 2.14. Detection of mtROS in RAW 264.7 cells and zebrafish larvae

RAW 264.7 macrophages were seeded at  $1 \times 10^5$  cells/ml in 8-well chamber slides, and DHP (0–25  $\mu$ M) was treated for 2 h prior to exposure to LPS (500 ng/mL). In parallel experiments MitoTEMPO (10  $\mu$ M) was treated 2 h before treatment with LPS (500 ng/mL). Then, the cells were stained with MitoTracker Green (0.5  $\mu$ M) for 30 min and counterstained with 2  $\mu$ M MitoSOX Red for 10 min [35]. In a parallel experiment, LPS (0.5 mg/mL, 2 nL in each larva) or PBS were microinjected in the yolk of 3 dpf zebrafish larvae and immediately immersed in embryo medium with DHP (25  $\mu$ M) and MitoTEMPO (10  $\mu$ M). At 18 hpi, the larvae were stained with 5  $\mu$ M MitoTracker Green for 30 min and continuous 10  $\mu$ M MitoSOX Red for 10 min [35]. Then, the larvae were anesthetized in 0.04% tricaine and fixed on methyl cellulose coated slides. Cell images were captured using a CELENA S Digital Imaging System (LogosBiosystems).

### 2.15. Measurement of mitochondrial membrane depolarization

RAW 264.7 macrophages were seeded at a density of  $1 \times 10^5$  cells/ml in a 6-well and treated with the indicated concentrations of DHP, MitoTEMPO (10  $\mu$ M), and TLR4-IN-C34 (10  $\mu$ M) for 2 h prior to exposure to LPS (500 ng/mL) for 2 h. Then, the cells were washed with ice-cold PBS and stained using a Muse MitoPotential Kit (Luminex) for 20 min [35]. Mitochondrial depolarization was measured by a Muse Cell Analyzer.

## 2.16. Statistical analysis

RT-PCR bands and western blot images were quantified using ImageJ (National Institute of Health, Bethesda, MD, USA, [www.imagej.net](http://www.imagej.net)). The results shown in each of figure are a representative from three independent experiments. The data was fit with a modified three parameter exponential decay using SigmaPlot Version 12.5 (Systat Software, San Jose, CA, USA, [www.systatsoftware.com](http://www.systatsoftware.com)). Significant differences between groups were determined using Student's t-test or one-way ANOVA with Bonferroni correction. Values were presented as standard error of the mean (SEM). \*\*\* and ###  $p < 0.001$ , \*\*  $p < 0.01$ , # and \*  $p < 0.05$  were considered to indicate statistical significance.

### 3. Results

#### 3.1. DHP decreases mortality and abnormality, and recovered the heart rate in LPS-microinjected zebrafish larvae

Zebrafish larvae were used as a model to study the effect of DHP on LPS microinjection-induced endotoxin shock. As shown in Table. 2, no morphological change was observed in PBS- or DHP-microinjected zebrafish larvae at 48 hpi; however, LPS microinjection caused 30% death and 55% abnormality, including swollen pericardial sac, cyrtosis, and yolk crenulation (Fig. 1.2A), in zebrafish larvae, and sustained 15% normality. Meanwhile, DHP decreased LPS microinjection-induced death and abnormality rate in a concentration-dependent manner. DHP at a concentration of 6.25  $\mu\text{M}$  decreased death rate to 15%, but slightly increased abnormality rate to 60%. In particular, DHP at concentrations of 12.5  $\mu\text{M}$  and 25  $\mu\text{M}$  completely inhibited mortality in LPS-microinjected zebrafish and significantly downregulated abnormality from 60% to 30% and 15%, respectively. In more detail, LPS microinjection caused 15% cyrtosis, 10% yolk crenulation, and 30% swollen pericardial sac in morphological abnormalities at 48 hpi. However, in LPS-microinjected zebrafish larvae in the presence of DHP at a concentration of 25  $\mu\text{M}$ , no yolk crenulation was observed, and 5% cyrtosis and 10% swollen pericardial sac were found (Fig. 1.2B). Furthermore, LPS microinjection caused a significant decrease of heart rates in zebrafish larvae at 24 hpi ( $143.4 \pm 1.2$  heartbeats/min) compared to that of PBS-microinjected larvae ( $181.8 \pm 1.5$  heartbeats/min, Fig. 2C). However, treatment with DHP gradually recovered the impaired heart rates to  $161.8 \pm 1.2$ ,  $180.5 \pm 1.2$ , and  $188.2 \pm 0.9$  heartbeats/min at 6.25, 12.5, and 25  $\mu\text{M}$ , respectively (Fig. 1.2C). These results indicate that DHP alleviates LPS-mediated endotoxic shock in zebrafish larvae.

Table 2 : Effects of DHP on mortality and abnormality in LPS-microinjected zebrafish

Treatment condition	Phenotypic ratio (%) (n=20)		
	Normality	Death	Abnormality
PBS	100	0	0
25 $\mu$ M DHP	100	0	0
LPS	15	30	55
6.25 $\mu$ M DPH + LPS	25	15	60
12.5 $\mu$ M DPH + LPS	70	0	30
25 $\mu$ M DPH + LPS	85	0	15

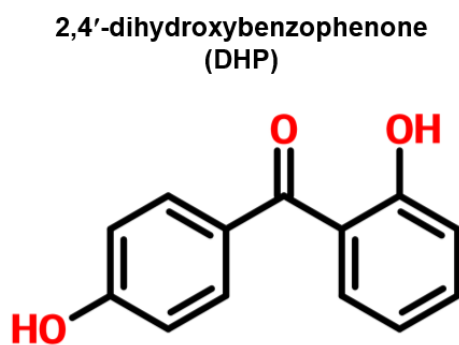
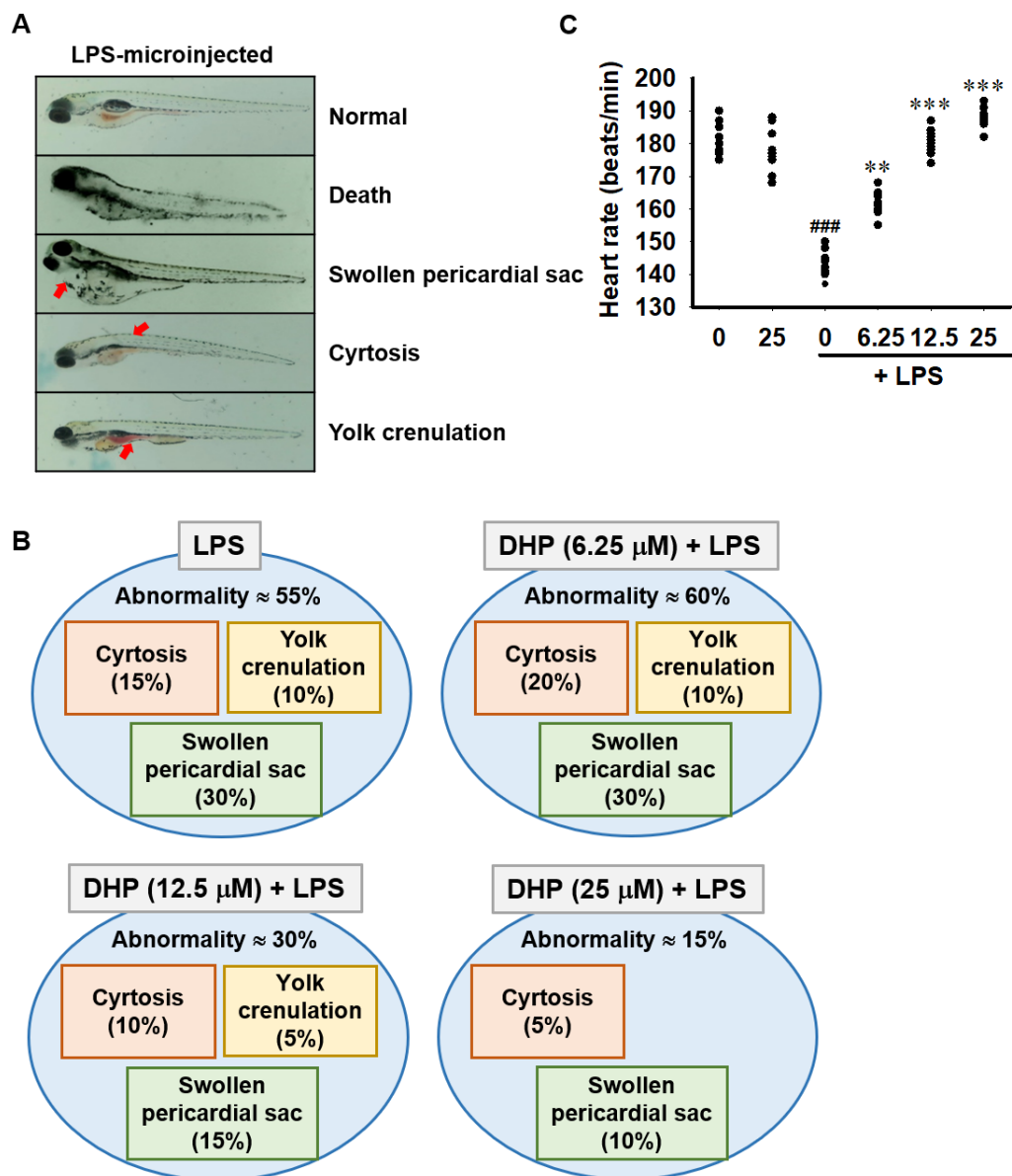


Fig. 1.1. Structure of 2,4'-dihydroxybenzophenone (DHP).



**Fig. 1.2.** DHP decreases mortality and abnormality in LPS-microinjected zebrafish larvae and recovers impaired heart rates. Zebrafish larvae at 3 days post-fertilization were microinjected with 2 nL of 0.5 mg/mL LPS and immediately immersed in the indicated concentrations of DHP (0–25  $\mu$ M). (A) LPS microinjection shows morphological abnormalities at 48 h post injection: death, swollen pericardial sac, cyrtosis, and yolk crenulation. Each characteristic was shown by a red arrow. (B) In the presence of DHP, proportion of LPS microinjection-mediated abnormality was calculated. (C) After 24 h post injection, heart rates were manually measured in 1 min. Each value indicates the mean  $\pm$  standard error median (SEM), and represent results



obtained from 20 fish for each group. Significant differences among groups were determined using Student's t-test (###  $p < 0.001$  vs. untreated zebrafish larvae) and one-way ANOVA with Bonferroni correction (\*\*  $p < 0.01$  and \*\*\*  $p < 0.001$  vs. LPS-microinjected zebrafish larvae).

### 3.2. DHP inhibits LPS-induced proinflammatory mediators in zebrafish larvae and decreases recruitment of macrophages and neutrophils to the infected sites

Because macrophages and neutrophils migrate to the inflammatory sites during an inflammatory response, we investigated whether DHP alleviates LPS-induced accumulation of macrophages and neutrophils using neutral red and sudan black staining. As shown in Fig. 1.3A, neutral red staining showed that DHP reduces the macrophage recruitment to the inflammatory site in a concentration-dependent manner (yolk sac). Sudan black staining also indicated that neutrophils are accumulated in the posterior blood island (PBI) area and disappear during LPS-microinjection, which indicates that neutrophils migrate from the PBI to the yolk sac in where LPS was microinjected (Fig. 1.3B). However, treatment with DHP markedly inhibited neutrophil migration to the inflammatory site and sustained neutrophils in the PBI area. Meanwhile, to evaluate anti-inflammatory effects of DHP, *iNOS*, *IL-12*, and *TNF- $\alpha$*  expression was investigated. Our results showed that LPS microinjection remarkably increases *iNOS*, *IL-12*, and *TNF- $\alpha$*  expression in zebrafish larvae at 18 hpi; however, the expression was gradually reduced in the presence of DHP (Fig. 1.3C). Therefore, our results indicate that DHP inhibits LPS-induced inflammatory response by downregulating proinflammatory gene expression and decreasing the migration of macrophage and neutrophil to the inflammatory site.

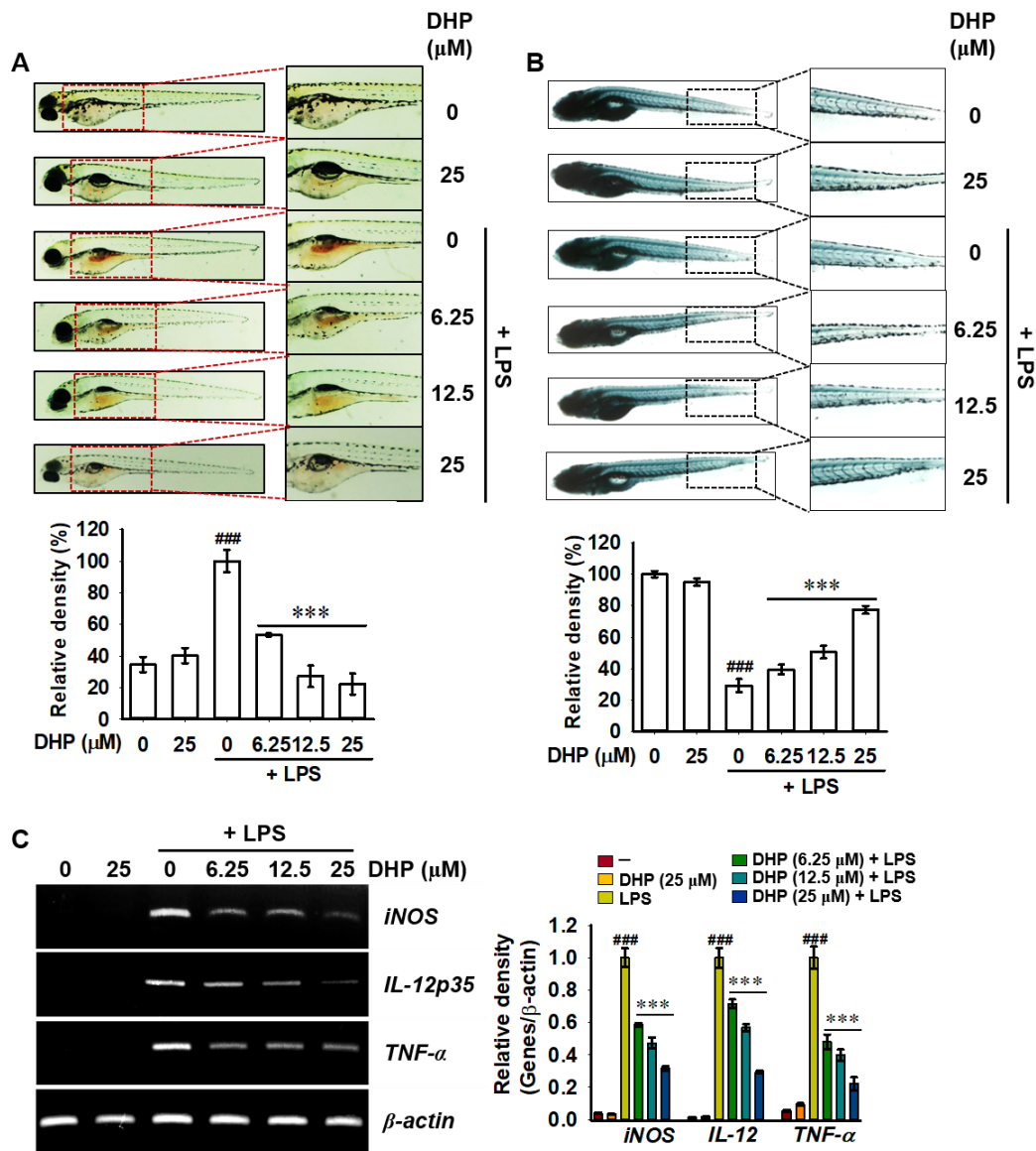


**Fig. 1.3.** DHP inhibits LPS-induced inflammatory responses in zebrafish larvae. Zebrafish larvae at 3 days post fertilization were microinjected with 2 nL of 0.5 mg/mL LPS into the yolk sac. Zebrafish larvae were immediately immersed in E3 embryo media containing DHP (0–25 μM). After 18 hours post injection (A) neutral red staining (macrophages) and (B) sudan black staining (neutrophils) were performed. (C) In a parallel experiment, zebrafish larvae were euthanized, and total RNA were extracted to perform RT-PCR to detect the expression levels of *iNOS*, *TNF-α*, and *IL-12p35*. β-Actin was used as an internal control for normalizing each gene expression. Significant differences among groups were determined using Student’s t-test

(###  $p < 0.001$  vs. untreated zebrafish larvae) and one-way ANOVA with Bonferroni correction  
(\* \*\*  $p < 0.001$  vs. LPS-microinjected zebrafish larvae).

### 3.3. High concentrations of DHP moderately decreases viability of RAW 264.7 macrophages

To investigate the effect of DHP on viability of RAW 264.7 macrophages, the cells were treated with the indicated concentrations of DHP for 24 h in the presence or absence of LPS. As shown in Fig. 1.4A, DHP at concentrations below 25  $\mu\text{M}$  did not significantly decrease the relative cell viability compared to that in untreated cells ( $98.1 \pm 2.6\%$ ,  $97.3 \pm 0.7\%$ ,  $98.0 \pm 0.2\%$  at 6.25, 12.5, and 25  $\mu\text{M}$  DHP, respectively). However, DHP at a concentration of 50  $\mu\text{M}$  moderately decreased the viability to  $69.2 \pm 0.6\%$ . LPS alone caused a decrease in cell viability ( $61.5 \pm 1.2\%$ ) by inducing differentiation of RAW 264.7 macrophages. Microscopic examination of cells treated with DHP did not show any floating cells, apoptotic bodies, or cell debris, even at 50  $\mu\text{M}$  (Fig. 1.4B). To confirm in detail the effect of DHP on viability of RAW 264.7 macrophages, total viable cell count and dead cell population were measured using flow cytometry. Consistent with MTT data, DHP at concentrations below 25  $\mu\text{M}$  did not decrease the viable cell counts,  $(3.4 \pm 0.0) \times 10^7$ ,  $(3.7 \pm 0.2) \times 10^7$ ,  $(3.6 \pm 0.1) \times 10^7$  cells/mL at 6.25, 12.5, and 25  $\mu\text{M}$ , respectively; however, DHP at a concentration of 50  $\mu\text{M}$  markedly downregulated the cell count to  $(2.6 \pm 0.2) \times 10^7$  cells/mL (Fig. 1.4C and 1.4D). In the presence of LPS, no significant difference was observed in viable cell count. Additionally, LPS-induced cell death was weakly downregulated at 25 and 50  $\mu\text{M}$  DHP (Fig. 1.4E). Therefore, DHP at concentrations below 25  $\mu\text{M}$  were used in further experiments.

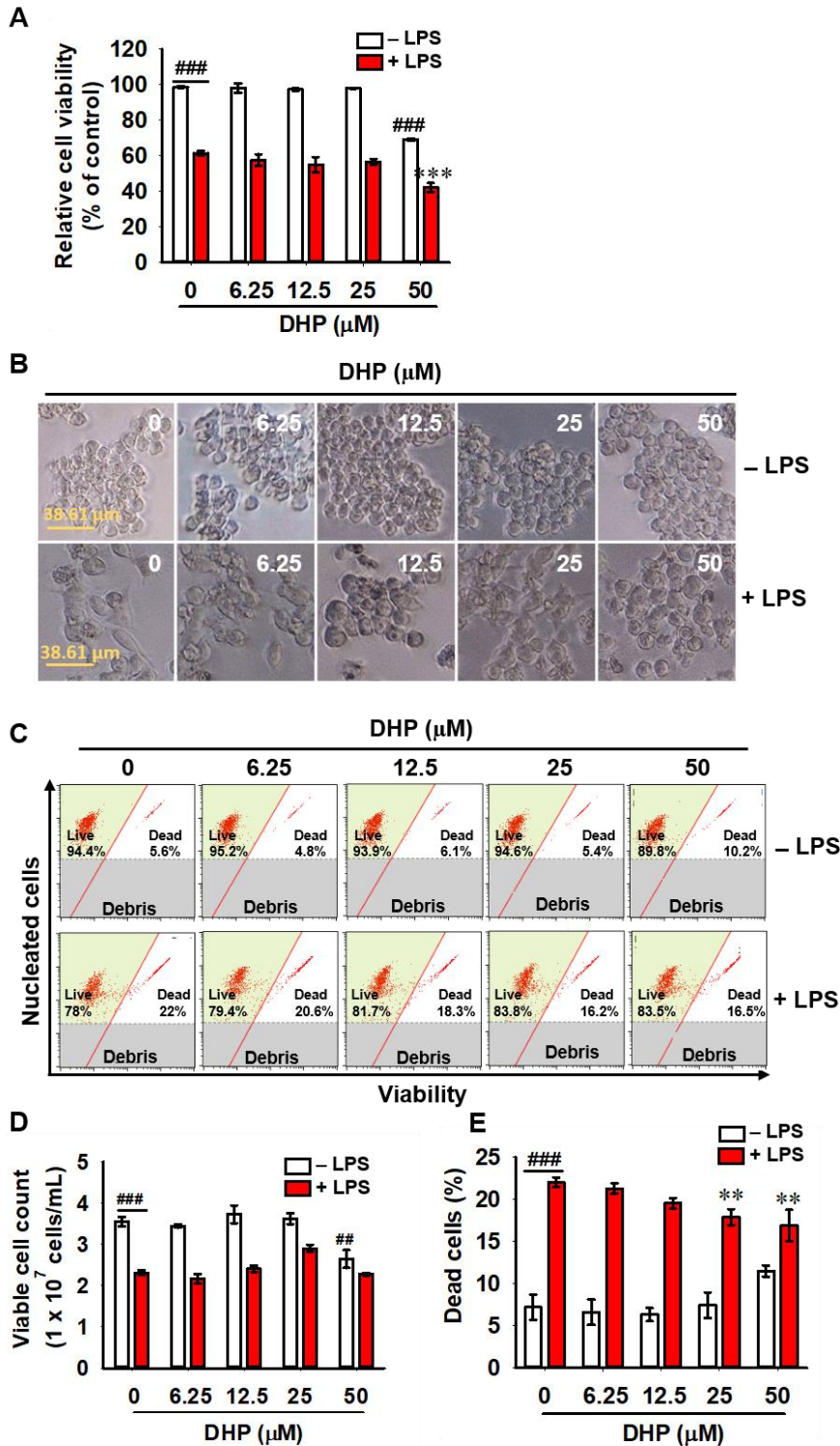


**Fig. 1.4.** A high concentration of DHP slightly gives damage in RAW 264.7 macrophages. RAW 264.7 macrophages ( $1 \times 10^5$  cells/mL) were treated with DHP (0–50  $\mu$ M) for 24h in the presence or absence of 500 ng/mL LPS. (A) Cell viability was measured using MTT assay. (B) Microscopic images were captured using phase-contrast microscopy ( $\times 10$ ). Scale bars (38.61

$\mu\text{m}$ ). (C) Total viable cell and dead cell population were determined using flow cytometry. (D) Viable cell count and (E) dead cell population were shown. Each value indicates the mean  $\pm$  SEM from three independent experiments. Significant differences among the groups were determined using Student's t-test and an unpaired one-way ANOVA with Bonferroni correction. ###  $p < 0.001$  and ##  $p < 0.01$  vs. untreated cells and \*\*\*  $p < 0.001$  vs. LPS-treated cells.

### 3.4. DHP inhibits LPS-induced proinflammatory mediators in RAW 264.7 macrophages

As shown in Fig. 5A, RT-PCR analysis revealed that LPS remarkably enhances expression of *iNOS*, *IL-12p35*, and *TNF- $\alpha$* , and DHP downregulated the expression in a concentration-dependent manner (Fig. 1.5A). LPS also increased NO production to  $16.6 \pm 0.4 \mu\text{M}$  compared to that in the untreated cells ( $1.1 \pm 0.1 \mu\text{M}$ ), and DHP significantly downregulated LPS-induced NO production to  $13.1 \pm 0.3$ ,  $10.8 \pm 0.4$ , and  $9.7 \pm 0.1 \mu\text{M}$  at 6.25, 12.5, and 25  $\mu\text{M}$ , respectively. (Fig. 1.5B). Moreover, ELISA results revealed that LPS treatment increased extracellular IL-12 production to  $1261.3 \pm 13.8 \text{ pg/mL}$  which is as much as 4-times higher than the untreated cells ( $288.0 \pm 7.5 \text{ pg/mL}$ ); however, DHP significantly decreased LPS-induced IL-12 production in a concentration-dependent manner ( $1072.4 \pm 12.5$ ,  $1022.7 \pm 5.6$ ,  $878.4 \pm 15.1 \text{ pg/mL}$  at 6.25, 12.5, and 25  $\mu\text{M}$ , respectively, Fig. 1.5C). Additionally, DHP ameliorated LPS-induced TNF- $\alpha$  production from  $1549.6 \pm 14.9 \text{ pg/mL}$  to  $1291.5 \pm 20.8$ ,  $1189.6 \pm 16.7$ , and  $897.0 \pm 9.8 \text{ pg/mL}$  at 6.25, 12.5, and 25  $\mu\text{M}$ , respectively (Fig. 1.5D). These results indicate that DHP could significantly downregulate LPS induced pro-inflammatory gene expressions and cytokine production in RAW 264.7 macrophages.



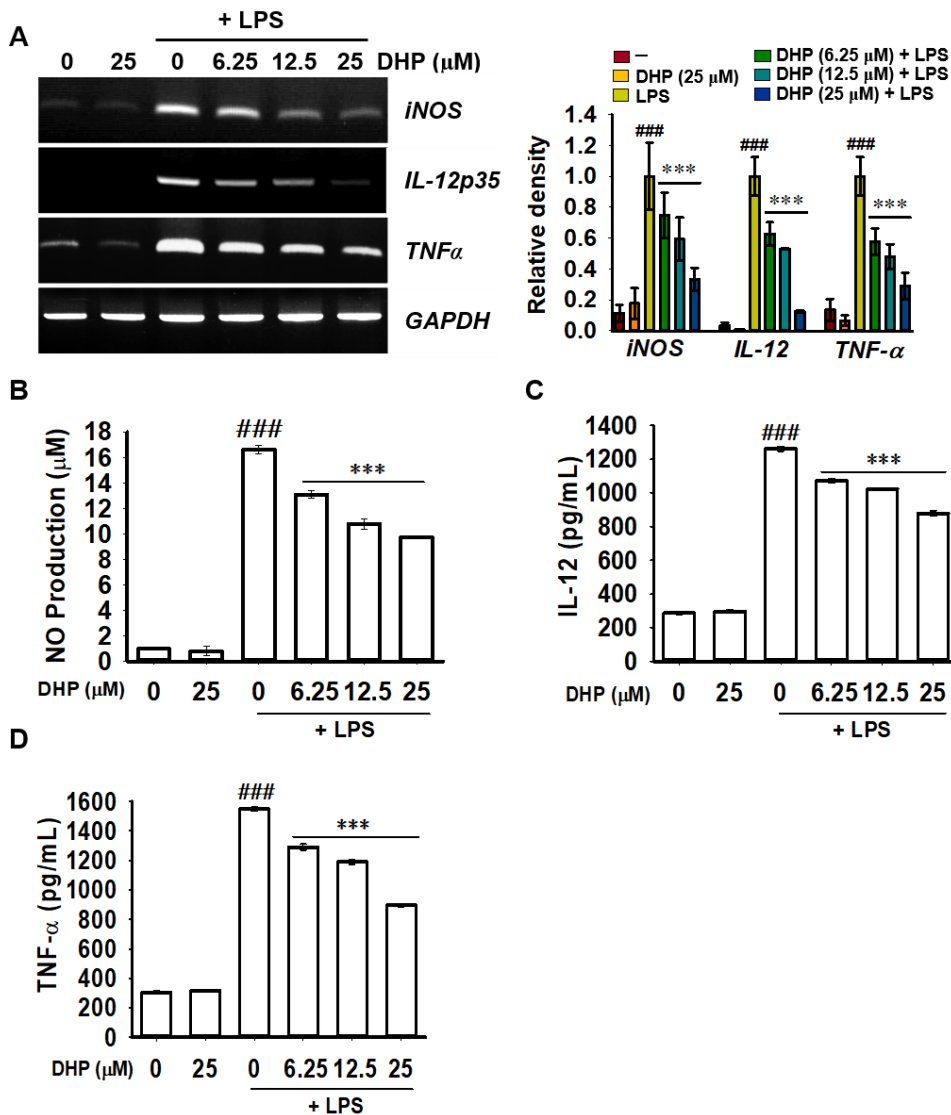


**Fig. 1.5.** DHP inhibits proinflammatory mediators in LPS-treated RAW 264.7 macrophages. RAW 264.7 macrophages ( $1 \times 10^5$  cells/ml) were treated with DHP (0–25  $\mu$ M) for 2 h followed by treatment with 500 ng/mL LPS. (A) Total mRNA was isolated 6 h after LPS treatment, and RT-PCR was performed for *iNOS*, *IL-12*, and *TNF- $\alpha$* . *GAPDH* was used as an internal control. The relative density was calculated using ImageJ, and each gene expression was normalized by the expression level of *GAPDH*. (B) Griess reagent assay was performed to assess NO production at 24 h after LPS treatment. The amount of (C) IL-12 and (D) TNF- $\alpha$  was measured using ELISA. Significant differences among the groups were determined using the Student's t-test and an unpaired one-way ANOVA with Bonferroni correction. ###  $p < 0.001$  vs. untreated cells, \*\*\*  $p < 0.001$  vs. LPS-treated cells.

### 3.5. DHP potentially binds to TLR4/MD2 receptor complex

To investigate whether DHP binds to TLR4/MD2 receptor complex, molecular docking prediction was performed. First, SwissDock simulation showed that DHP could bind to mouse and human TLR/MD2 receptor complex (PDB ID: 3VQ1 and 3FXI, respectively) at 52 and 65 clusters (binding sites), respectively (Supplementary Table 1 and Table 2). Approximately 66% and 56% clusters in 3VQ1 (pink 'a' in Fig. 1.6A and 1.6B) and 3FXI (pink 'a' Fig. 1.7A and 1.7B) predicted to bind the MD2 pocket where lipid parts fit into. Besides, some minor elements were also found (pink 'b-f' in Fig. 1.6A and 1.6B, and pink 'b-e' Fig. 1.7A and 1.7B). The strongest binding estimated  $\Delta G$ s of DHP were -6.52 with 3VQ1 and -6.57 kcal/mol with 3FXI. Additionally, in consistence with SwissDock data, mcule docking study also showed that DHP strongly fits into the hydrophobic pocket of MD2 at -7.6 binding score with 3VQ1 (Fig. 1.6C and 1.6D) and at -6.6 binding score with 3FXI (Fig. 1.7C and 1.7D); however, discrete hydrogen bonding was not found with the TLR4/MD2 receptor complex. 2D protein-ligand binding models showed that DHP forms many different non-covalent bonds with MD2, such as vander Waals,  $\pi$ - $\pi$  stacked,  $\pi$ -alkyl interactions (Fig. 1.6E and Fig. 1.7E).  $\pi$ -Sigma and  $\pi$ -sulfur interactions were discovered with 3VQ1 and 3FXI, respectively. The data indicate that DHP fits into the hydrophobic pocket of MD2 and inhibits TLR4-mediated inflammatory signaling pathway.

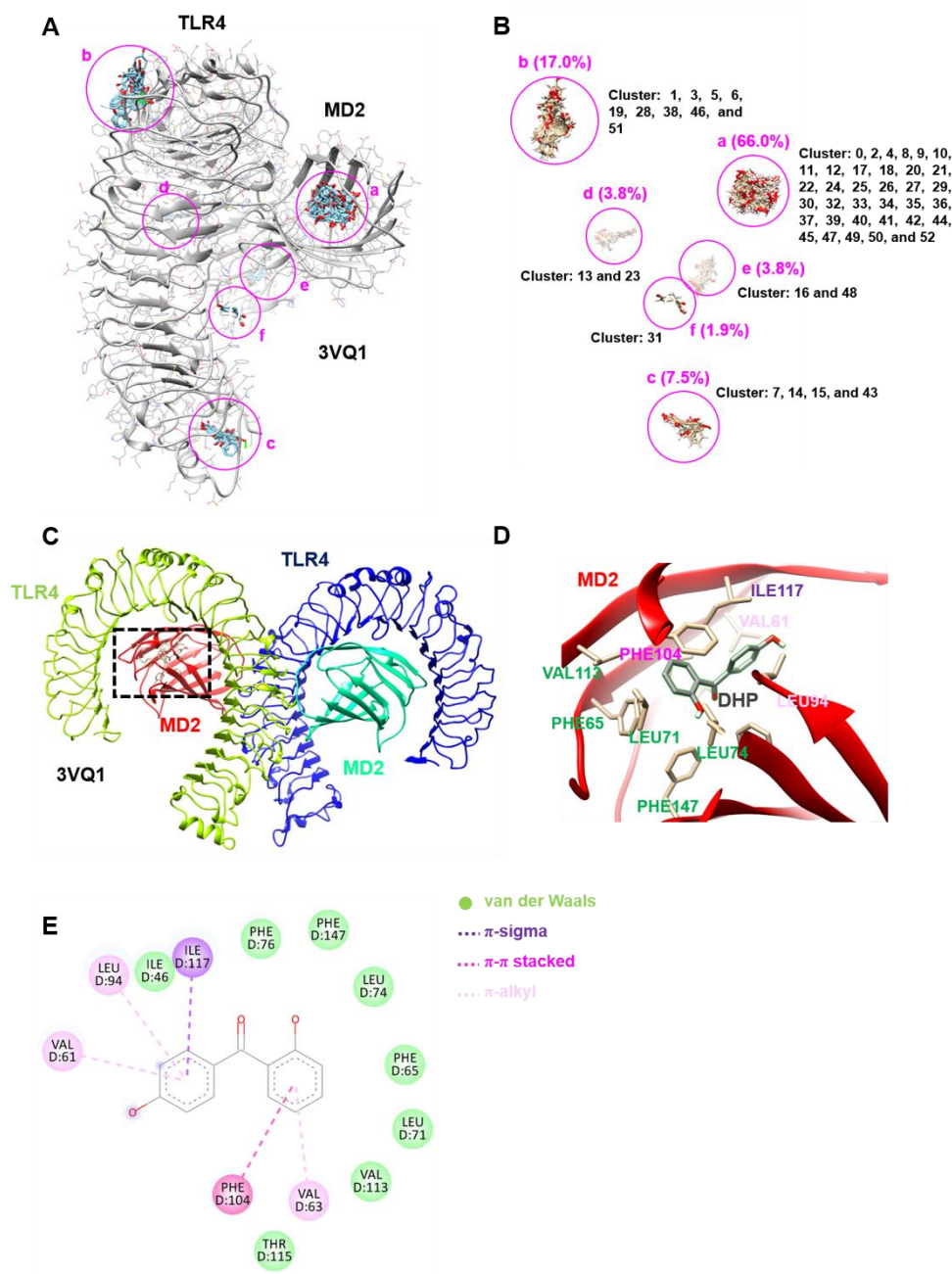


**Fig. 1.6.** DHP possibly binds to mouse TLR4/MD2 receptor complex (3VQ1). (A and B) All possible binding positions were predicted using SwissDock. (C) Using mcule, the strongest binding pose between DHP and 3VQ1 was shown. (D) Black dotted square in (C) were enlarged and amino acids were marked around DHP. (E) The 2D binding analysis shows non-covalent interactions between DHP and 3VQ1.

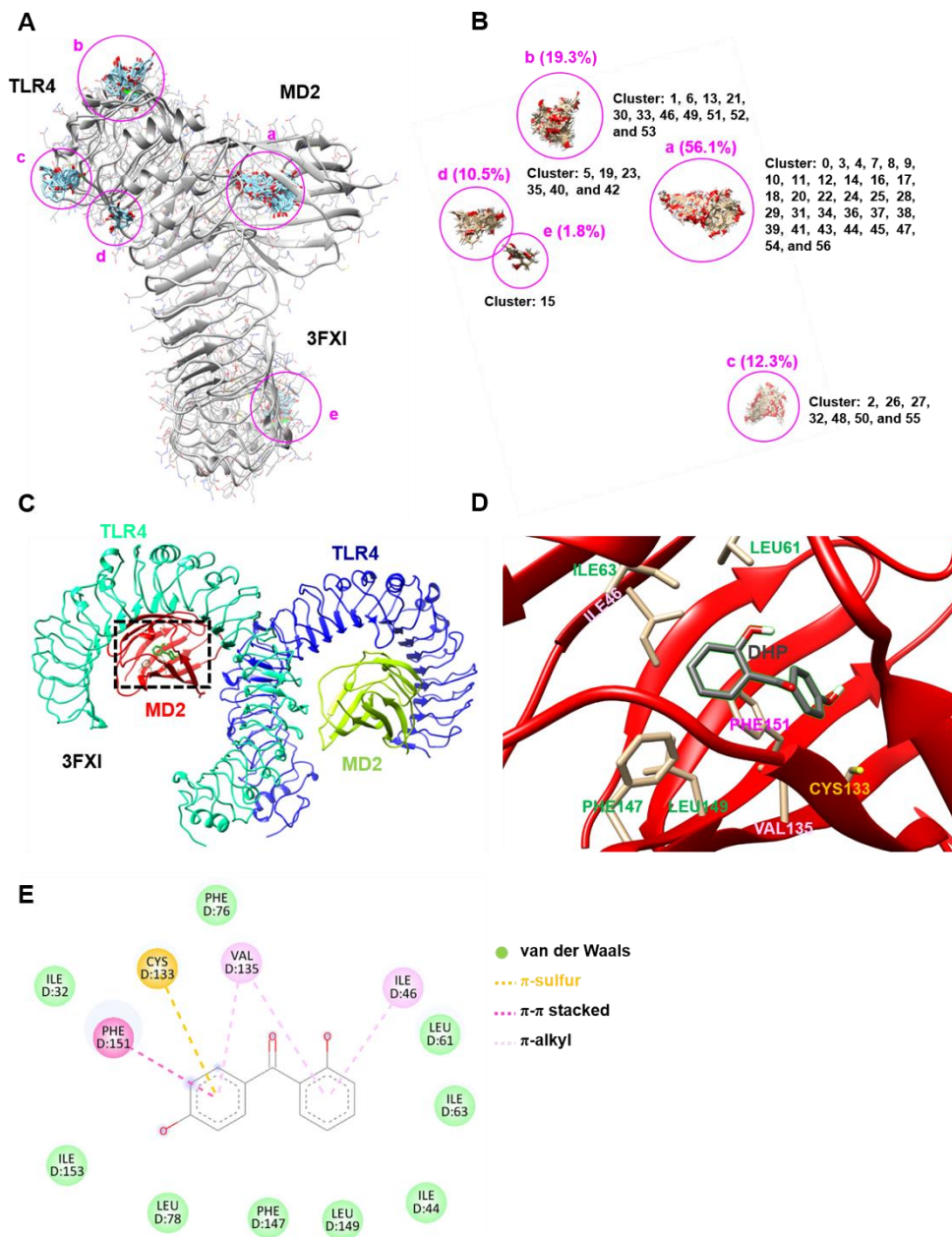


**Fig. 1.7.** DHP possibly binds to human TLR4/MD2 receptor complex (3FXI). DHP possibly binds to human TLR4/MD2 receptor complex (3FXI). (A and B) All possible binding positions were predicted using SwissDock. (C) Using mcule, the strongest binding pose between DHP and 3FXI was shown. (D) Black dotted square in (C) were enlarged and amino acids were marked around DHP. (E) The 2D binding analysis shows non-covalent interactions between DHP and 3FXI.

### *3.6. DHP inhibits the MyD88-IRAK4-NF- $\kappa$ B signaling pathway*

To confirm whether binding of DHP to the TLR4/MD2 receptor complex inhibits TLR4-mediated intracellular signaling pathway, we treated RAW 264.7 macrophages with DHP in the presence or absence of LPS and investigated TLR4 expression on the cell membrane and intracellular signaling pathway. Immunostaining results indicated that DHP attenuates TLR4 expression or dimerization (Fig. 1.8A). Western blotting data showed that DHP inhibits LPS-induced MyD88 expression and IRAK4 phosphorylation which are related to NF- $\kappa$ B activation (Fig. 1.8B). Because endotoxin finally target NF- $\kappa$ B-mediated inflammatory gene expression via the TLR4/MD2 receptor complex [7], we investigated whether DHP inhibits nuclear translocation of NF- $\kappa$ B subunits, such as p50 and p65. Western blot analysis showed that DHP inhibits LPS-induced nuclear translocation of NF- $\kappa$ B p50 and p65 subunits in a concentration-dependent manner (Fig. 1.8C). Immunostaining data also confirmed that DHP reduced LPS-induced nuclear translocation of NF- $\kappa$ B p65 (Fig. 1.8D). The data confirm that DHP inhibits TLR4 dimerization and consequently prevents TLR4-mediated inflammatory signaling pathway by suppressing the MyD88-IRAK4-NF- $\kappa$ B signaling pathway.

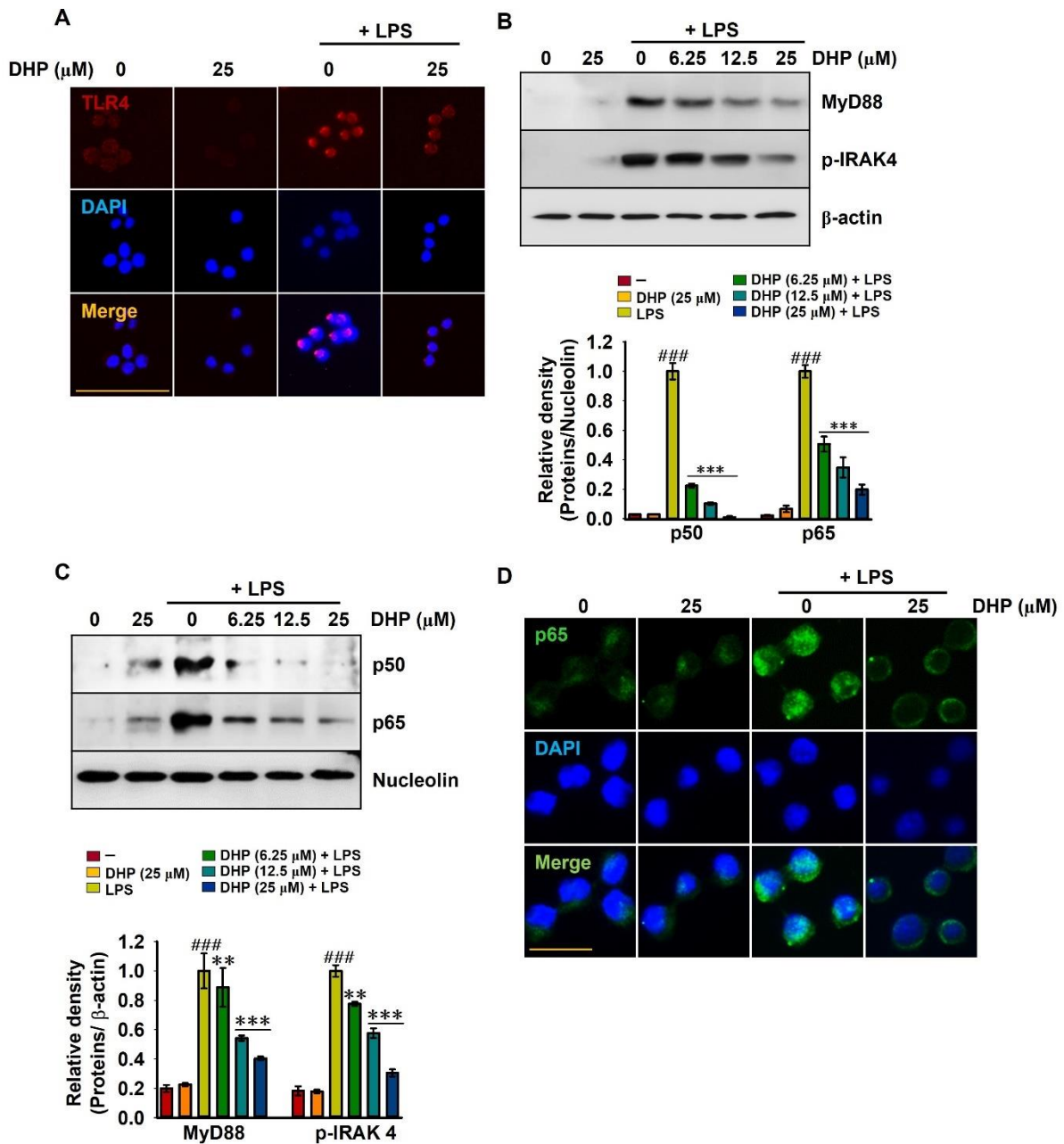


**Fig. 1.8.** DHP inhibits TLR4 expression and the MyD88-IRAK4-NF- $\kappa$ B signaling pathway. (A) RAW 264.7 macrophages were treated with 25  $\mu\text{M}$  DHP for 2 h prior to 500 ng/mL LPS treatment and immunostained with anti-TLR4 antibody and Alexa Fluor 488-conjugated secondary antibody followed by nuclear counterstaining with DAPI. Fluorescence images were captured using a CELENA S digital imaging system. Scale bar: 75  $\mu\text{m}$ . (B) Cytosolic proteins were isolated for western blotting.  $\beta$ -Actin was used as an internal control for normalizing MyD88 and IRAK4 expression. (C) Nuclear proteins were extracted for western blotting.

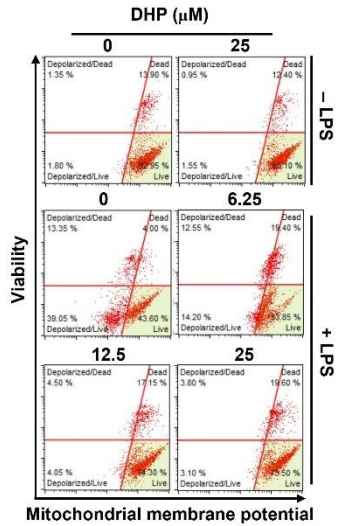
Nucleolin was used as an internal control for normalizing p50 and p65 expression. (D) RAW 264.7 macrophages were treated with 25  $\mu$ M DHP for 2 h prior to 500 ng/mL LPS treatment and immunostained with anti-p65 antibody and Alexa Fluor 488-conjugated secondary antibody followed by nuclear counterstaining with DAPI. Fluorescence images were captured using a CELENA S digital imaging system. Scale bar: 25  $\mu$ m. Each value indicates the mean  $\pm$  standard error median (SEM), and representative of results obtained from three independent experiments. Significant differences among the groups were determined using the Student's t-test and an unpaired one-way ANOVA with Bonferroni correction. ###  $p < 0.001$  vs. untreated cells; \*\*\*  $p < 0.001$  and \*\*  $p < 0.01$  vs. LPS-treated cells.

### *3.7. DHP decreases LPS-induced mitochondrial membrane depolarization and mtROS production in RAW 264.7 macrophages*

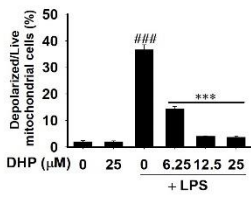
We, next, determined the effect of DHP on mitochondrial membrane depolarization and mtROS production in RAW 264.7 macrophages. According to the results, DHP itself did not affect the alteration of mitochondrial membrane depolarization; however, depolarized live mitochondrial cell populations exhibiting depolarized mitochondrial membrane potential were significantly increased to  $36.7 \pm 2.0\%$  in LPS-treated RAW 264.7 macrophages. Moreover, DHP decreased the depolarized live mitochondrial cell populations in a concentration-dependent manner and the highest concentration significantly downregulated the depolarized live cells to  $3.7 \pm 0.3\%$ , similar to the levels in untreated ( $2.0 \pm 0.4\%$ , Fig. 1.9A). In a parallel experiment, immunofluorescence staining data demonstrated that in LPS-treated RAW 264.7 macrophages, Mitotracker (a fluorescent dye specific for mitochondria) MitoSOX Red (a fluorescent dye specific for mtROS) glowed at the merged site, which indicates that LPS dramatically stimulates mtROS production (Fig. 1.9B). We also found that DHP treatment decreases LPS-induced mtROS production in RAW 264.7 macrophages (Fig. 1.9B). To examine whether mtROS production boosts intracellular TLR4/MD2 signaling pathway via the MyD88-IRAK4- NF- $\kappa$ B axis, RAW 264.7 macrophages were treated with LPS in the presence of MitoTEMPO, a mitochondria-targeted antioxidant, and mtROS production and intracellular signaling pathways were investigated. As expected, MitoTEMPO dramatically alleviated total cell populations possessing depolarized mitochondria membrane potential from  $19.7 \pm 0.3\%$  to  $13.0 \pm 0.9\%$  (Fig. 1.9C) and mtROS production (Fig. 1.9D) in LPS-treated RAW 264.7 macrophages. Additionally, our results showed that MitoTEMPO decreases LPS-induced MyD88 and p-IRAK4 expression (Fig. 1.9E), and nuclear translocation of p50 and p65 subunits upon LPS stimulation (Fig. 1.9F). The results indicate that DHP inhibits LPS-induced inflammatory signaling pathway by suppressing mtROS production.



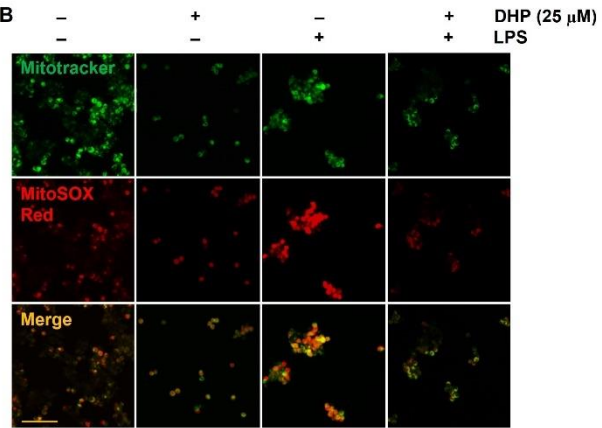
**A**



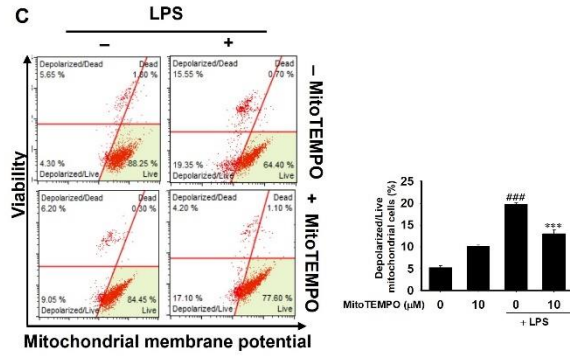
Mitochondrial membrane potential



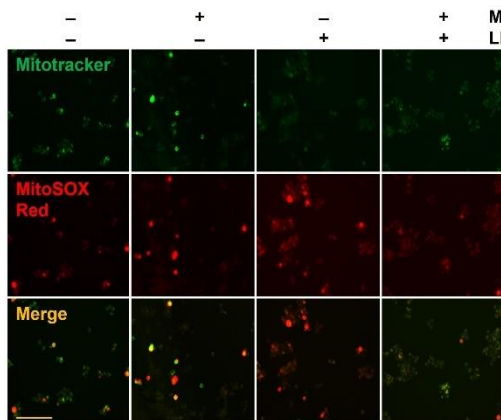
**B**



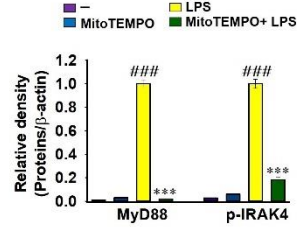
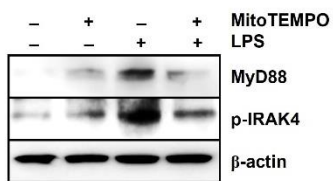
**C**



**D**



**E**



**F**

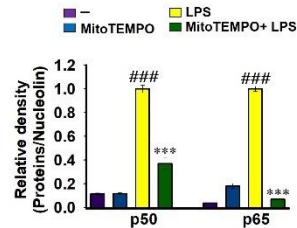
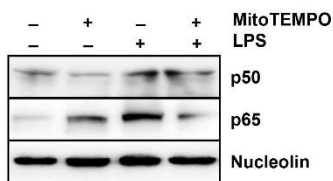


**Fig. 1.9.** DHP inhibits LPS-induced mitochondrial membrane potential depolarization and mtROS production. RAW 264.7 macrophages ( $1 \times 10^5$  cells/ml) were treated with DHP (0–25  $\mu$ M) or MitoTEMPO (10  $\mu$ M) for 2h prior to treatment with 500 ng/mL LPS for 2 h. (A and C) The cells were stained using a Muse MitoPotential Kit, and mitochondrial membrane depolarization was analyzed using flow cytometry. Total depolarized mitochondrial cells were represented. (B and D) The cells were stained with 0.5  $\mu$ M MitoTracker Green for 30 min followed by 2  $\mu$ M MitoSOX Red for 10 min. Immunofluorescence staining was performed, and images were captured using a CELENA S Digital Imaging System. Scale bar: 100  $\mu$ m. (E) Cytosolic and (F) nuclear proteins were extracted for western blotting.  $\beta$ -Actin and nucleolin were used as cytosolic and nuclear internal controls, respectively. Each value indicates the mean  $\pm$  standard error median, and representative of results obtained from three independent experiments. Significant differences among the groups were determined using the Student's t-test and an unpaired one-way ANOVA with Bonferroni correction. ####  $p < 0.001$  vs. untreated cells; \*\*  $p < 0.01$  and \*\*\*  $p < 0.001$  vs. LPS-treated cells.

### 3.8. DHP decreases LPS-induced mtROS production in zebrafish larvae

To investigate inhibition of LPS-induced mtROS production *in vivo* by DHP, zebrafish at 3 dpf were microinjected with LPS and immersed in E3 media containing DHP or MitoTEMPO for 24 h. The heart rate evaluation indicated that LPS-microinjected zebrafish have a significant decrease in heart rate ( $133.0 \pm 1.6$  heartbeats/min) compared to that of PBS-microinjected larvae ( $175.5 \pm 1.7$  heartbeats/min). However, treatment with both DHP or MitoTEMPO recovered the decreased heart rate caused by LPS microinjection ( $175.5 \pm 1.7$  and  $161.8 \pm 1.2$  heart beats/min, respectively, Fig. 1.10A), which indicates that inhibition of mtROS production restores decreased heart rate in endotoxin shock. Additionally, immunofluorescent staining indicated that treatment with both DHP or MitoTEMPO dramatically alleviated LPS microinjection-induced mtROS production in zebrafish larvae (Fig. 1.10B). Therefore, our results confirm that DHP alleviates LPS-induced mtROS production *in vivo* and restores the heart rate.

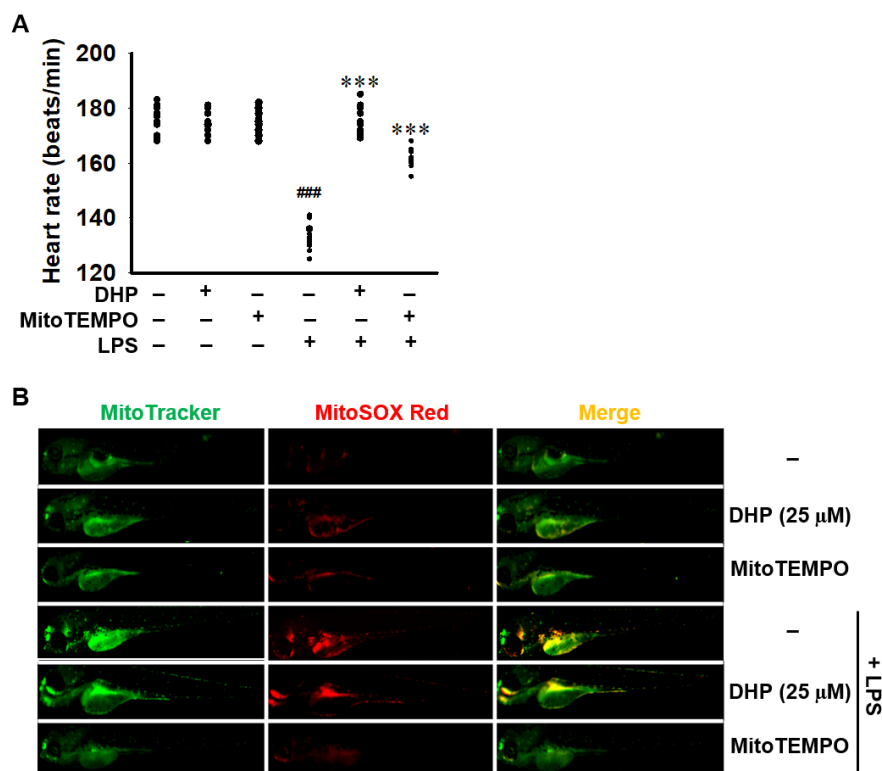


**Fig. 1.10.** DHP decreases mtROS production and restores the heart rate in LPS-microinjected zebrafish larvae. Zebrafish at 3 days post fertilization were microinjected with 2 nL of 0.5 mg/mL LPS into the yolk sac. The larvae were immediately immersed in E3 embryo media containing DHP (25  $\mu$ M) or MitoTEMPO (10  $\mu$ M). (A) At 24 h post injection, the heart rates were manually measured in 1 min. (B) Zebrafish larvae were stained with 0.5  $\mu$ M MitoTracker for 30 min followed by 2  $\mu$ M MitoSOX Red for 10 min. Immunofluorescent staining was performed, and images were captured using a CELENA S Digital Imaging System. Each value indicates the mean  $\pm$  standard error median, and representative of results obtained from three independent experiments. Significant differences among the groups were determined using the Student's t-test and an unpaired one-way ANOVA with Bonferroni correction. ###  $p < 0.001$  vs. PBS-microinjected zebrafish larvae; \*\*\*  $p < 0.001$  vs. LPS-microinjected zebrafish larvae.

3.9. DHP potently binds with TLR4 and alleviate mitochondrial depolarization in RAW 264.7 macrophages

To investigate how DHP could alleviate mitochondrial depolarization upon LPS treatment, we treated 25  $\mu\text{M}$  DHP 2 hours prior to LPS treatment for another 2 hours. At the same time a known TLR4 inhibitor (TLR4-IN-C34) was treated 2 hours prior to LPS treatment for another 2 hours. According to our results DHP could decrease LPS induced total depolarized mitochondrial cell percentage from  $20.2 \pm 0.6\%$  to  $9.7 \pm 1.2\%$ . Interestingly, TLR4 inhibitor also decreased LPS induced total depolarized mitochondrial cell percentage to  $10.3 \pm 0.3\%$  (Fig. 1.11). These results indicate that DHP could bind with TLR4 and alleviate mitochondrial depolarization in RAW 264.7 macrophages.

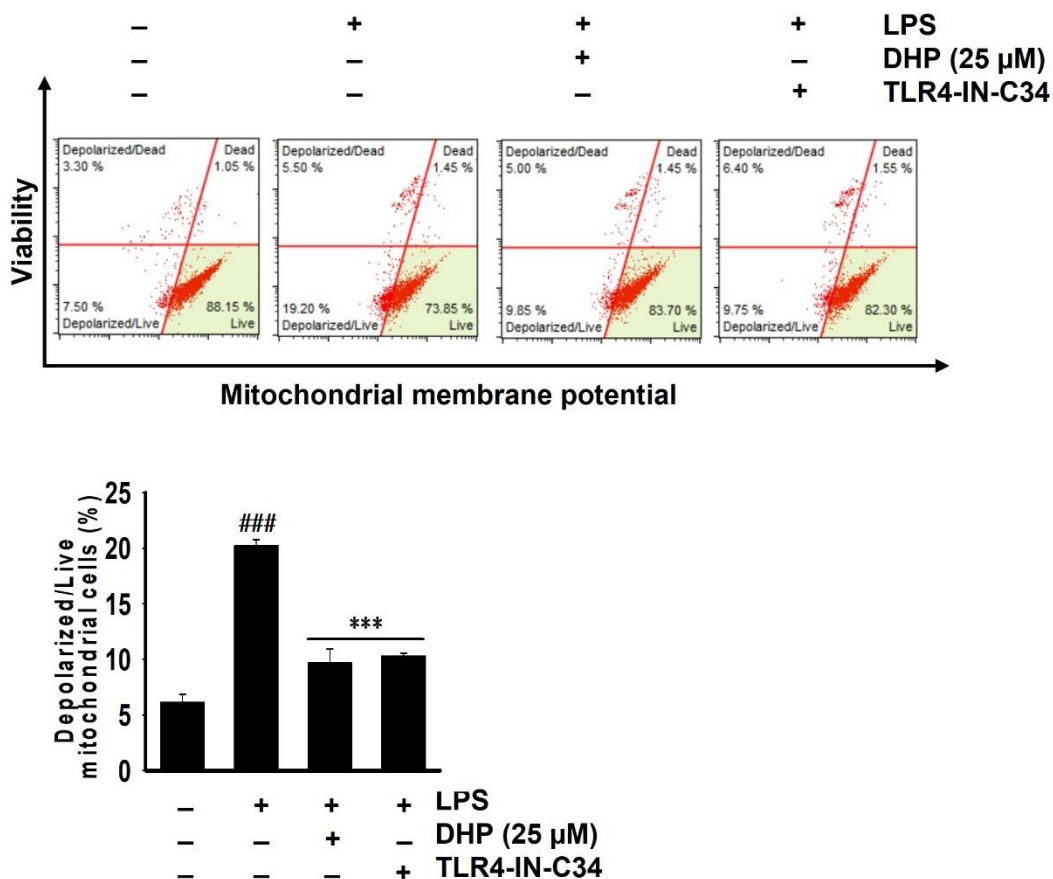


**Fig. 1.11.** Inhibition of TLR4 signaling reduces LPS-induced mitochondrial membrane potential depolarization. RAW 264.7 macrophages ( $1 \times 10^5$  cells/ml) were treated with DHP

(25  $\mu$ M) or TLR4-IN-C34 (10  $\mu$ M) for 2 h prior to 500 ng/mL LPS treatment for another 2 h. Cells were stained using a Muse MitoPotential Kit, and mitochondrial membrane potential depolarization was analyzed using flow cytometry. Significant differences among the groups were determined using the Student's t-test and an unpaired one-way ANOVA with Bonferroni correction. ###  $p < 0.001$  vs. untreated cells; \*\*\*  $p < 0.001$  vs. LPS-treated cells.

#### 4. Discussion

Endotoxic shock is induced by endotoxins which are produced by the outer membrane of gram-negative bacteria and serves as a systemically life-threatening inflammatory response [1, 2]. Endotoxic shock is marked by fever, hypotension, dyspnea, and multiple organ dysfunctions, finally causing a high mortality rate over approximately 40% [5, 29]. Nevertheless, Admilk et al. described that elimination of endotoxin using hemoperfusion effectively improved hemodynamic parameters and organ function in intensive care unit (ICU) patients with septic shock but does not show a significant effect on ICU mortality [36]. The observational study indicates that LPS removal from blood circulation cannot reduce endotoxin shock-mediated mortality after LPS transfers inflammatory response through the MyD88-IRAK4-NF- $\kappa$ B axis. In the regard, Shapiro et al. reviewed that small compounds such as polyphenols have been highlighted in the prevention and treatment of sepsis by enhancing the endogenous antioxidant capacity, such as the Nrf-HO-1 axis [37]. In this study, we found that DPH possibly binds to the TLR4/MD2 receptor complex and inhibits severe inflammatory responses, such as endotoxin shock, both in vitro and in vivo.

LPS can highly stimulates macrophages to induce endotoxin shock by excessive release of pro-inflammatory mediators such as NO, TNF- $\alpha$ , and IL-12 [38, 39]. In particular, IL-12 is a macrophage-derived cytokine and play an important role in endotoxin shock through stimulation of interferon- $\gamma$  from T cells, and potent suppression of IL-12 production blunts endotoxin tolerance [40, 41]. Because TNF- $\alpha$  is responsible for acute phase of inflammation and septic shock [24], Ashkenzazi et al. determined that soluble TNF receptor (TNFR) or anti-TNFR-Ig efficeiently prevents endotoxin-induced lethality and suggest a clinical potential for targeting TNFR inhibition [42]. The role of NO in sepsis is still contradictory in favorable and detrimental actions. Wright et al. confirmed that in the condition of endotoxin shock, inhibition of both constitutive NOS and iNOS is detrimental; however, selective inhibition of iNOS is

beneficial to inhibit endotoxin shock [43]. Through meta-analysis of controlled clinical trials, Pascual-Ramirez and Koutrouvelis determined that NO antagonists are effective to septic shock and increase adverse effects [44], insisting that use of NO antagonists is difficult depending on the timely treatment. In this study, our results revealed that DHP significantly downregulates LPS-induced proinflammatory mediators such as NO, TNF- $\alpha$ , and IL-12, resulting in the inhibition of mortality and abnormality, and restoration of heartbeat in an endotoxin shock model. Nevertheless, whether DHP prevents low blood pressure and multiorgan failure in endotoxin shock should be investigated.

Toll-like receptors (TLRs) are important in initiating inflammatory response since LPS binds to the TLR4/MD2 receptor complex and triggers intracellular signaling pathway through the MyD88-IRAK4-NF- $\kappa$ B axis [6, 7]. Finally, NF- $\kappa$ B is responsible for the production of proinflammatory mediators such as NO, TNF- $\alpha$ , and IL-12, and plays an crucial role in the pathophysiology of endotoxin shock [45]. mtROS is also essential to organ injury in endotoxin shock accompanied by depolarization of mitochondrial membrane potential, and TLR4 inhibitors and antioxidants ameliorate organ failure in endotoxin shock by inhibiting mtROS production [14, 15, 46]. Hence, targeting NF- $\kappa$ B and mtROS is an important therapeutic strategy for preventing and treating LPS-induced inflammatory disorders [47]. More recently, many phytochemicals and molecules targeting the TLR4/MD2 receptor complex provides successful therapeutics with efficient safety and pharmacokinetics in preclinical and clinical trials [48, 49]. In particular, phytochemicals specifically targeting TLR4/MD2 complex fit in the hydrophobic pocket and occludes the binding of TLR4 and MD2, which prevents many inflammatory disorders, including endotoxin shock, in experimental models [50-52]. In molecular docking study, we found that DHP can fit in the hydrophobic pocket of MD2 and prevent LPS binding to the TLR4/MD2 receptor complex, which attenuates mtROS production. In this regard, DHP may be a potential therapeutic candidate for endotoxin shock. Nevertheless,



in this study, after LPS microinjection, zebrafish immediately immersed in media containing DHP, which indicates that the zebrafish were almost simultaneously exposed to LPS and DHP, and DHP may compete with LPS for binding to TLR4/MD2 receptor complex. In this case, DHP was effective to inhibit endotoxin shock accompanied by inhibition of mtROS production. However, it is questionable whether DHP is still effective in the endotoxin shock induced after long-term LPS exposure, because LPS first activates inflammatory signals via the TLR4/MD2 complex.

In conclusion, in this study, we demonstrated that DHP alleviates LPS-induced endotoxin shock by inhibiting the TLR4/MD2 signaling pathway. Additionally, antioxidant capacity of DHP simultaneously reduced mtROS production and restored mitochondrial membrane potential. Therefore, our data indicate that DHP as a mitochondria-targeting antioxidant could alleviate LPS-induced endotoxin shock.

## 5. References

1. Cecconi, M.; Evans, L.; Levy, M.; Rhodes, A., Sepsis and septic shock. *Lancet* **2018**, 392, (10141), 75-87.
2. Opal, S. M., Endotoxins and other sepsis triggers. *Contrib Nephrol* **2010**, 167, 14-24.
3. Khan, H. N.; Perlee, D.; Schoenmaker, L.; van der Meer, A. J.; Franitza, M.; Toliat, M. R.; Nurnberg, P.; Zwinderman, A. H.; van der Poll, T.; Scicluna, B. P., Leukocyte transcriptional signatures dependent on LPS dosage in human endotoxemia. *J Leukoc Biol* **2019**, 106, (5), 1153-1160.
4. Kim, S. J.; Kim, H. M., Dynamic lipopolysaccharide transfer cascade to TLR4/MD2 complex via LBP and CD14. *BMB Rep* **2017**, 50, (2), 55-57.
5. Park, B. S.; Lee, J. O., Recognition of lipopolysaccharide pattern by TLR4 complexes. *Exp Mol Med* **2013**, 45, (12), e66.
6. Guven-Maiorov, E.; Keskin, O.; Gursoy, A.; VanWaes, C.; Chen, Z.; Tsai, C. J.; Nussinov, R., The Architecture of the TIR Domain Signalosome in the Toll-like Receptor-4 Signaling Pathway. *Sci Rep* **2015**, 5, 13128.
7. Fitzgerald, K. A.; Kagan, J. C., Toll-like Receptors and the Control of Immunity. *Cell* **2020**, 180, (6), 1044-1066.
8. Hawkins, L. D.; Christ, W. J.; Rossignol, D. P., Inhibition of endotoxin response by synthetic TLR4 antagonists. *Curr Top Med Chem* **2004**, 4, (11), 1147-71.
9. Jang, J. C.; Li, J.; Gambini, L.; Batugedara, H. M.; Sati, S.; Lazar, M. A.; Fan, L.; Pellecchia, M.; Nair, M. G., Human resistin protects against endotoxic shock by blocking LPS-TLR4 interaction. *Proc Natl Acad Sci U S A* **2017**, 114, (48), E10399-E10408.

10. Brand, M. D.; Orr, A. L.; Perevoshchikova, I. V.; Quinlan, C. L., The role of mitochondrial function and cellular bioenergetics in ageing and disease. *Br J Dermatol* **2013**, 169 Suppl 2, (0 2), 1-8.
11. Canton, M.; Sanchez-Rodriguez, R.; Spera, I.; Venegas, F. C.; Favia, M.; Viola, A.; Castegna, A., Reactive Oxygen Species in Macrophages: Sources and Targets. *Front Immunol* **2021**, 12, 734229.
12. Galley, H. F., Oxidative stress and mitochondrial dysfunction in sepsis. *Br J Anaesth* **2011**, 107, (1), 57-64.
13. Nagar, H.; Piao, S.; Kim, C. S., Role of Mitochondrial Oxidative Stress in Sepsis. *Acute Crit Care* **2018**, 33, (2), 65-72.
14. Cimolai, M. C.; Alvarez, S.; Bode, C.; Bugger, H., Mitochondrial Mechanisms in Septic Cardiomyopathy. *Int J Mol Sci* **2015**, 16, (8), 17763-78.
15. Victor, V. M.; Espulgues, J. V.; Hernandez-Mijares, A.; Rocha, M., Oxidative stress and mitochondrial dysfunction in sepsis: a potential therapy with mitochondria-targeted antioxidants. *Infect Disord Drug Targets* **2009**, 9, (4), 376-89.
16. Kong, X.; Thimmulappa, R.; Kombairaju, P.; Biswal, S., NADPH oxidase-dependent reactive oxygen species mediate amplified TLR4 signaling and sepsis-induced mortality in Nrf2-deficient mice. *J Immunol* **2010**, 185, (1), 569-77.
17. Tomasi, M. L.; Ryoo, M.; Yang, H.; Iglesias Ara, A.; Ko, K. S.; Lu, S. C., Molecular mechanisms of lipopolysaccharide-mediated inhibition of glutathione synthesis in mice. *Free Radic Biol Med* **2014**, 68, 148-58.
18. Lei, L.; Chai, Y.; Lin, H.; Chen, C.; Zhao, M.; Xiong, W.; Zhuang, J.; Fan, X., Dihydroquercetin Activates AMPK/Nrf2/HO-1 Signaling in Macrophages and Attenuates Inflammation in LPS-Induced Endotoxemic Mice. *Front Pharmacol* **2020**, 11, 662.

19. Dorman, G.; Prestwich, G. D., Benzophenone photophores in biochemistry. *Biochemistry* **1994**, 33, (19), 5661-73.
20. Cuquerella, M. C.; Lhiaubet-Vallet, V.; Cadet, J.; Miranda, M. A., Benzophenone photosensitized DNA damage. *Acc Chem Res* **2012**, 45, (9), 1558-70.
21. Zhang, Y.; Shah, P.; Wu, F.; Liu, P.; You, J.; Goss, G., Potentiation of lethal and sub-lethal effects of benzophenone and oxybenzone by UV light in zebrafish embryos. *Aquat Toxicol* **2021**, 235, 105835.
22. Cui, F.; Pan, Q.; Wang, S.; Zhao, F.; Wang, R.; Zhang, T.; Song, Y.; He, J.; Zhang, H.; Weng, Q.; Jin, Y.; Xia, W.; Li, Y.; Yang, G. Y.; De Vos, W. H.; Timmermans, J. P.; Xu, S.; Tang, Y.; Sheng, X., Maternal Benzophenone Exposure Impairs Hippocampus Development and Cognitive Function in Mouse Offspring. *Adv Sci (Weinh)* **2021**, 8, (23), e2102686.
23. Huang, C. Y.; Chang, T. C.; Wu, Y. J.; Chen, Y.; Chen, J. J., Benzophenone and Benzoylphloroglucinol Derivatives from *Hypericum sampsonii* with Anti-Inflammatory Mechanism of Otogirin A. *Molecules* **2020**, 25, (19).
24. Kang, Y.; Sun, Y.; Li, T.; Ren, Z., Garcinol protects against cerebral ischemia-reperfusion injury in vivo and in vitro by inhibiting inflammation and oxidative stress. *Mol Cell Probes* **2020**, 54, 101672.
25. Che Hassan, N. K. N.; Taher, M.; Susanti, D., Phytochemical constituents and pharmacological properties of *Garcinia xanthochymus*- a review. *Biomed Pharmacother* **2018**, 106, 1378-1389.
26. Giustarini, D.; Rossi, R.; Milzani, A.; Dalle-Donne, I., Nitrite and nitrate measurement by Griess reagent in human plasma: evaluation of interferences and standardization. *Methods Enzymol* **2008**, 440, 361-80.

27. Karunarathne, W.; Lee, K. T.; Choi, Y. H.; Jin, C. Y.; Kim, G. Y., Anthocyanins isolated from *Hibiscus syriacus* L. attenuate lipopolysaccharide-induced inflammation and endotoxic shock by inhibiting the TLR4/MD2-mediated NF-kappaB signaling pathway. *Phytomedicine* **2020**, *76*, 153237.
28. Ohto, U.; Fukase, K.; Miyake, K.; Shimizu, T., Structural basis of species-specific endotoxin sensing by innate immune receptor TLR4/MD-2. *Proc Natl Acad Sci U S A* **2012**, *109*, (19), 7421-6.
29. Park, B. S.; Song, D. H.; Kim, H. M.; Choi, B. S.; Lee, H.; Lee, J. O., The structural basis of lipopolysaccharide recognition by the TLR4-MD-2 complex. *Nature* **2009**, *458*, (7242), 1191-5.
30. Bitencourt-Ferreira, G.; de Azevedo, W. F., Jr., Docking with SwissDock. *Methods Mol Biol* **2019**, *2053*, 189-202.
31. Kiss, R.; Szalai, F.; Sandor, M., Mcule.com: A public web service for drug discovery. *Abstr Pap Am Chem S* **2012**, 243.
32. Pettersen, E. F.; Goddard, T. D.; Huang, C. C.; Couch, G. S.; Greenblatt, D. M.; Meng, E. C.; Ferrin, T. E., UCSF Chimera--a visualization system for exploratory research and analysis. *J Comput Chem* **2004**, *25*, (13), 1605-12.
33. Menu Neelaka Molagoda, I.; Arachchilage Hasitha Maduranga Karunarathne, W.; Lee, M. H.; Kang, C. H.; Tae Lee, K.; Hyun Choi, Y.; Lee, S.; Kim, G. Y., Acertannin attenuates LPS-induced inflammation by interrupting the binding of LPS to the TLR4/MD2 complex and activating Nrf2-mediated HO-1 activation. *Int Immunopharmacol* **2022**, *113*, (Pt A), 109344.
34. Athapaththu, A.; Lee, K. T.; Kavinda, M. H. D.; Lee, S.; Kang, S.; Lee, M. H.; Kang, C. H.; Choi, Y. H.; Kim, G. Y., Pinostrobin ameliorates lipopolysaccharide (LPS)-

- induced inflammation and endotoxemia by inhibiting LPS binding to the TLR4/MD2 complex. *Biomed Pharmacother* **2022**, 156, 113874.
35. Molagoda, I. M. N.; Athapaththu, A.; Choi, Y. H.; Park, C.; Jin, C. Y.; Kang, C. H.; Lee, M. H.; Kim, G. Y., Fisetin Inhibits NLRP3 Inflammasome by Suppressing TLR4/MD2-Mediated Mitochondrial ROS Production. *Antioxidants (Basel)* **2021**, 10, (8).
36. Adamik, B.; Zielinski, S.; Smiechowicz, J.; Kubler, A., Endotoxin Elimination in Patients with Septic Shock: An Observation Study. *Arch Immunol Ther Exp (Warsz)* **2015**, 63, (6), 475-83.
37. Shapiro, H.; Lev, S.; Cohen, J.; Singer, P., Polyphenols in the prevention and treatment of sepsis syndromes: rationale and pre-clinical evidence. *Nutrition* **2009**, 25, (10), 981-97.
38. Reis, J.; Guan, X. Q.; Kisselev, A. F.; Papasian, C. J.; Qureshi, A. A.; Morrison, D. C.; Van Way, C. W., 3rd; Vogel, S. N.; Qureshi, N., LPS-induced formation of immunoproteasomes: TNF-alpha and nitric oxide production are regulated by altered composition of proteasome-active sites. *Cell Biochem Biophys* **2011**, 60, (1-2), 77-88.
39. Soufli, I.; Toumi, R.; Raza, H.; Touil-Boukoffa, C., Overview of cytokines and nitric oxide involvement in immuno-pathogenesis of inflammatory bowel diseases. *World J Gastrointest Pharmacol Ther* **2016**, 7, (3), 353-60.
40. Karp, C. L.; Wysocka, M.; Ma, X.; Marovich, M.; Factor, R. E.; Nutman, T.; Armant, M.; Wahl, L.; Cuomo, P.; Trinchieri, G., Potent suppression of IL-12 production from monocytes and dendritic cells during endotoxin tolerance. *Eur J Immunol* **1998**, 28, (10), 3128-36.

41. Li, C. C.; Munitic, I.; Mittelstadt, P. R.; Castro, E.; Ashwell, J. D., Suppression of Dendritic Cell-Derived IL-12 by Endogenous Glucocorticoids Is Protective in LPS-Induced Sepsis. *PLoS Biol* **2015**, 13, (10), e1002269.
42. Ashkenazi, A.; Marsters, S. A.; Capon, D. J.; Chamow, S. M.; Figari, I. S.; Pennica, D.; Goeddel, D. V.; Palladino, M. A.; Smith, D. H., Protection against endotoxic shock by a tumor necrosis factor receptor immunoadhesin. *Proc Natl Acad Sci U S A* **1991**, 88, (23), 10535-9.
43. Wright, C. E.; Rees, D. D.; Moncada, S., Protective and pathological roles of nitric oxide in endotoxin shock. *Cardiovasc Res* **1992**, 26, (1), 48-57.
44. Pascual-Ramirez, J.; Koutrouvelis, A., The nitric oxide pathway antagonists in septic shock: Meta-analysis of controlled clinical trials. *J Crit Care* **2019**, 51, 34-38.
45. Liu, S. F.; Malik, A. B., NF-kappa B activation as a pathological mechanism of septic shock and inflammation. *Am J Physiol Lung Cell Mol Physiol* **2006**, 290, (4), L622-L645.
46. Li, Y.; Feng, G., TLR4 inhibitor alleviates sepsis-induced organ failure by inhibiting platelet mtROS production, autophagy, and GPIIb/IIIa expression. *J Bioenerg Biomembr* **2022**, 54, (3), 155-162.
47. Giridharan, S.; Srinivasan, M., Mechanisms of NF-kappaB p65 and strategies for therapeutic manipulation. *J Inflamm Res* **2018**, 11, 407-419.
48. Hernandez-Jimenez, M.; Martin-Vilchez, S.; Ochoa, D.; Mejia-Abril, G.; Roman, M.; Camargo-Mamani, P.; Luquero-Bueno, S.; Jilma, B.; Moro, M. A.; Fernandez, G.; Pineiro, D.; Ribo, M.; Gonzalez, V. M.; Lizasoain, I.; Abad-Santos, F., First-in-human phase I clinical trial of a TLR4-binding DNA aptamer, ApTOLL: Safety and pharmacokinetics in healthy volunteers. *Mol Ther Nucleic Acids* **2022**, 28, 124-135.

49. Anwar, M. A.; Shah, M.; Kim, J.; Choi, S., Recent clinical trends in Toll-like receptor targeting therapeutics. *Med Res Rev* **2019**, 39, (3), 1053-1090.
50. Dai, W.; Long, L.; Wang, X.; Li, S.; Xu, H., Phytochemicals targeting Toll-like receptors 4 (TLR4) in inflammatory bowel disease. *Chin Med* **2022**, 17, (1), 53.
51. Saleh, H. A.; Yousef, M. H.; Abdelnaser, A., The Anti-Inflammatory Properties of Phytochemicals and Their Effects on Epigenetic Mechanisms Involved in TLR4/NF-kappaB-Mediated Inflammation. *Front Immunol* **2021**, 12, 606069.
52. Molteni, M.; Bosi, A.; Rossetti, C., Natural Products with Toll-Like Receptor 4 Antagonist Activity. *Int J Inflamm* **2018**, 2018, 2859135



## Appendix

**Supplementary Table 1.** Analysis of binding activity between DHP and 3VQ1 using SwissDock.

Cluster	Element	FullFitness (kcal/mol)	Estimated G (kcal/mol)	Cluster	Element	FullFitness (kcal/mol)	Estimated G (kcal/mol)	Cluster	Element	FullFitness (kcal/mol)	Estimated G (kcal/mol)
0	0	-3323.21	-6.52	10	0	-3320.14	-6.33	28	0	-3317.37	-6.09
0	1	-3323.21	-6.52	11	0	-3320.06	-6.23	28	1	-3317.33	-6.06
0	2	-3323.21	-6.52	11	1	-3320.06	-6.23	28	2	-3317.27	-6.12
0	3	-3323.21	-6.52	11	2	-3320.06	-6.23	28	3	-3317.26	-6.11
0	4	-3323.1	-6.51	11	3	-3320.06	-6.23	28	4	-3316.7	-6.04
0	5	-3322.54	-6.46	11	4	-3320.06	-6.23	28	5	-3316.3	-5.97
0	6	-3322.33	-6.44	11	5	-3320.06	-6.23	29	0	-3317.34	-6.17
0	7	-3322.2	-6.41	11	6	-3319.26	-6.16	29	1	-3317.32	-6.28
0	8	-3322.2	-6.41	11	7	-3319.23	-6.16	29	2	-3316.6	-6.16
0	9	-3321.96	-6.4	11	8	-3316.3	-6.16	29	3	-3315.58	-6.06
0	10	-3321.26	-6.38	12	0	-3319.55	-6.16	29	4	-3313.95	-6.15
0	11	-3321.15	-6.33	12	1	-3319.41	-6.14	29	5	-3313.81	-6.13
0	12	-3321.14	-6.33	13	0	-3319.41	-6.29	30	0	-3317.34	-5.98
0	13	-3321.14	-6.33	13	1	-3319.41	-6.3	30	1	-3317.34	-5.98
0	14	-3320.1	-6.29	13	2	-3319.41	-6.29	30	2	-3313.37	-5.82
1	0	-3322	-6.63	13	3	-3319.33	-6.28	30	3	-3313.36	-5.82
1	1	-3319.8	-6.28	13	4	-3317.4	-6.11	30	4	-3313.36	-5.82
1	2	-3319.41	-6.48	13	5	-3316.98	-6.04	30	5	-3312.87	-5.75
1	3	-3318.89	-6.41	13	6	-3315.22	-5.96	30	6	-3312.83	-5.75
1	4	-3318.15	-6.52	13	7	-3314.69	-5.9	30	7	-3312.78	-5.74
1	5	-3317.13	-6.16	14	0	-3319.04	-6.08	31	0	-3317.11	-5.93

1	6	-3310.95	-5.54	14	1	-3319.02	-6.07	31	1	-3317.11	-5.93
1	7	-3308.7	-5.74	14	2	-3312.2	-5.9	31	2	-3317.11	-5.93
2	0	-3321.85	-6.43	15	0	-3318.91	-6.08	31	3	-3317.1	-5.95
2	1	-3319.34	-6.32	15	1	-3316.86	-6.19	31	4	-3317.1	-5.95
2	2	-3319.07	-6.17	16	0	-3318.73	-6.32	31	5	-3317.1	-5.95
2	3	-3318.9	-6.18	16	1	-3318.72	-6.31	31	6	-3317.1	-5.95
2	4	-3318.58	-6.2	16	2	-3314.27	-5.92	31	7	-3317.1	-5.95
2	5	-3318.42	-6.12	16	3	-3308.67	-5.72	32	0	-3317.11	-6.06
2	6	-3317.86	-6.36	16	4	-3308.1	-5.78	32	1	-3317.11	-6.06
2	7	-3317.83	-6.34	16	5	-3307.1	-5.51	32	2	-3316.81	-6.03
2	8	-3317.09	-6.04	16	6	-3303.88	-5.58	32	3	-3316.81	-6.03
2	9	-3316.98	-6.01	17	0	-3318.69	-6.16	32	4	-3316.55	-6.01
2	10	-3316.58	-5.99	17	1	-3317.71	-6.07	32	5	-3314.03	-5.88
3	0	-3321.75	-7.02	17	2	-3317.66	-6.08	32	6	-3313.98	-5.88
3	1	-3321.75	-7.02	17	3	-3316.95	-6.04	32	7	-3313.98	-5.88
3	2	-3320.7	-6.91	17	4	-3316.93	-6.04	33	0	-3316.79	-6.15
3	3	-3318.49	-6.7	17	5	-3314.18	-6.01	33	1	-3316.78	-6.15
3	4	-3318.45	-6.69	18	0	-3318.68	-6.32	33	2	-3316.78	-6.15
3	5	-3318.26	-6.67	18	1	-3318	-6.24	33	3	-3316.78	-6.15
3	6	-3318.26	-6.67	18	2	-3317.14	-6.21	33	4	-3316.78	-6.15
3	7	-3312.15	-6.14	18	3	-3315.71	-5.91	33	5	-3316.78	-6.15
4	0	-3321.14	-6.4	18	4	-3315.26	-6.02	33	6	-3316.78	-6.15
4	1	-3321.14	-6.4	18	5	-3312.54	-5.91	33	7	-3316.78	-6.15
4	2	-3321.14	-6.4	19	0	-3318.49	-6.32	34	0	-3316.72	-6.21
4	3	-3321.14	-6.4	19	1	-3318.49	-6.32	34	1	-3316.72	-6.21
4	4	-3321.14	-6.4	19	2	-3318.49	-6.32	34	2	-3316.53	-6.19
4	5	-3321.14	-6.41	19	3	-3318.49	-6.32	34	3	-3316.53	-6.19

4	6	-3321.14	-6.41	19	4	-3318.42	-6.31	34	4	-3316.53	-6.19
4	7	-3321.14	-6.41	19	5	-3318.42	-6.31	34	5	-3316.5	-6.19
5	0	-3321.01	-6.67	19	6	-3318.42	-6.31	34	6	-3316.5	-6.19
5	1	-3321.01	-6.67	19	7	-3318.42	-6.31	34	7	-3316.5	-6.19
5	2	-3321	-6.67	20	0	-3318.42	-6.16	35	0	-3316.47	-6.03
5	3	-3321	-6.67	20	1	-3317.79	-6.28	36	0	-3316.25	-5.98
5	4	-3321	-6.67	20	2	-3317.79	-6.28	36	1	-3314.93	-6
5	5	-3321	-6.67	20	3	-3317.78	-6.27	36	2	-3314.12	-5.86
5	6	-3321	-6.67	21	0	-3318.32	-6.23	37	0	-3316.12	-5.88
5	7	-3321	-6.67	22	0	-3318.3	-6.04	37	1	-3315.38	-5.98
6	0	-3320.57	-6.64	22	1	-3318.06	-6.18	37	2	-3315.38	-5.98
6	1	-3320.56	-6.64	22	2	-3317.94	-6.19	38	0	-3316.08	-6.43
6	2	-3315.11	-6.06	22	3	-3316.57	-6.08	39	0	-3315.82	-5.95
6	3	-3310.95	-5.83	23	0	-3318.21	-6.06	40	0	-3315.77	-5.85
6	4	-3309.06	-5.61	23	1	-3318.21	-6.06	41	0	-3315.18	-5.91
7	0	-3320.48	-6.25	23	2	-3318.2	-6.06	41	1	-3313.92	-5.87
7	1	-3320.48	-6.25	23	3	-3318.2	-6.06	42	0	-3315.08	-6.03
7	2	-3320.47	-6.25	23	4	-3315.8	-6.06	43	0	-3315.01	-5.7
7	3	-3320.47	-6.25	23	5	-3315.8	-6.06	43	1	-3310.98	-5.76
7	4	-3320.47	-6.25	23	6	-3315.8	-6.07	43	2	-3310.77	-5.8
7	5	-3320.47	-6.25	23	7	-3315.76	-6.06	44	0	-3314.84	-5.96
7	6	-3320.47	-6.25	24	0	-3317.93	-6.06	45	0	-3314.41	-5.88
7	7	-3320.47	-6.25	24	1	-3317.9	-6.05	46	0	-3313.99	-6
8	0	-3320.2	-6.26	24	2	-3317.88	-6.05	47	0	-3313.76	-5.98
8	1	-3318.08	-6.09	24	3	-3316.56	-6.09	47	1	-3313.58	-6.01
8	2	-3317.61	-6.08	25	0	-3317.86	-5.98	48	0	-3312.59	-6.12
8	3	-3316.69	-6.21	25	1	-3317.71	-5.96	49	0	-3311.36	-5.71

8	4	-3316.67	-6.2	25	2	-3317.71	-5.99	50	0	-3310.72	-5.59
9	0	-3320.18	-6.32	25	3	-3317.53	-5.96	51	0	-3310.26	-5.78
9	1	-3318.67	-6.07	25	4	-3316.85	-5.94	51	1	-3310.09	-5.94
9	2	-3318.42	-5.99	25	5	-3316.25	-5.88	51	2	-3309.87	-5.83
9	3	-3318.04	-5.95	26	0	-3317.77	-6.01	52	0	-3307.25	-5.87
9	4	-3317.88	-6.13	26	1	-3317.06	-5.99	52	0	-3307.25	-5.87
9	5	-3317.78	-5.96	26	2	-3317.06	-5.99				
9	6	-3317.48	-5.98	26	3	-3317.06	-5.99				
9	7	-3317.22	-6.13	26	4	-3314.92	-6.01				
9	8	-3316.93	-5.95	26	5	-3314.83	-6.01				
9	9	-3316.27	-5.81	27	0	-3317.72	-6.09				
9	10	-3316.09	-6.1	27	1	-3316.98	-6				
9	11	-3313.39	-5.94								
9	12	-3312.32	-5.82								

**Supplementary Table 2.** Analysis of binding activity between DPH and 3FXI using SwissDock.

Cluster	Element	FullFitness (kcal/mol)	Estimated G (kcal/mol)	Cluster	Element	FullFitness (kcal/mol)	Estimated G (kcal/mol)	cluster	Element	FullFitness (kcal/mol)	Estimated G (kcal/mol)
0	0	-3398.6	-6.57	14	0	-3395.32	-6.38	30	0	-3394.65	-6.44
0	1	-3395.23	-6.4	14	1	-3395.31	-6.38	30	1	-3392.8	-6.28
0	2	-3395.2	-6.47	14	2	-3392.84	-6.42	31	0	-3394.57	-6.22
0	3	-3395.17	-6.47	14	3	-3389.79	-6.13	31	1	-3394.55	-6.21
1	0	-3397.23	-6.71	14	4	-3388.88	-6.06	31	2	-3394.53	-6.22
2	0	-3397.01	-6.68	15	0	-3395.26	-6.31	31	3	-3394.28	-6.22
2	1	-3396.53	-6.58	15	1	-3395.05	-6.28	31	4	-3391.69	-6.15
2	2	-3395.8	-6.49	15	2	-3394.71	-6.36	31	5	-3391.67	-6.15
2	3	-3395.56	-6.68	15	3	-3394.71	-6.36	31	6	-3391.67	-6.16
2	4	-3395.53	-6.67	15	4	-3394.71	-6.36	31	7	-3391.39	-6.12
2	5	-3395.3	-6.46	15	5	-3394.61	-6.31	32	0	-3394.55	-6.53
2	6	-3394.86	-6.6	15	6	-3394.61	-6.31	33	0	-3394.34	-6.34
2	7	-3394.41	-6.37	15	7	-3393.01	-6.02	33	1	-3394.17	-6.34
2	8	-3394.29	-6.35	16	0	-3395.23	-6.18	33	2	-3394.14	-6.3
2	9	-3391.64	-6.44	16	1	-3395.11	-6.21	33	3	-3390.55	-6.16
2	10	-3387.53	-6.08	16	2	-3394.83	-6.4	33	4	-3390.39	-6.16
2	11	-3387.41	-6.13	16	3	-3393.28	-6.24	33	5	-3390.19	-6.13
3	0	-3396.5	-6.44	16	4	-3393.24	-6.25	33	6	-3387.73	-6.15
3	1	-3396.48	-6.46	16	5	-3392.15	-6.24	33	7	-3387.7	-6.14
3	2	-3394.8	-6.31	16	6	-3392.08	-6.24	34	0	-3394.28	-6.31
3	3	-3394.2	-6.22	17	0	-3395.22	-6.48	34	1	-3394.28	-6.31
3	4	-3394	-6.23	17	1	-3395.22	-6.48	34	2	-3387.55	-6.16
3	5	-3392.37	-6.21	17	2	-3395.22	-6.48	34	3	-3387.54	-6.16

3	6	-3391.69	-6.06	17	3	-3395.15	-6.48	34	4	-3386.8	-5.9
3	7	-3390.63	-6.08	17	4	-3395.15	-6.48	34	5	-3386.72	-6.01
4	0	-3396.38	-6.47	17	5	-3395.15	-6.48	35	0	-3393.58	-6.48
4	1	-3396	-6.31	17	6	-3394.68	-6.38	35	1	-3393.58	-6.48
4	2	-3395.23	-6.61	17	7	-3394.68	-6.38	35	2	-3393.56	-6.46
4	3	-3394.54	-6.36	18	0	-3395.22	-6.25	35	3	-3393.42	-6.48
4	4	-3392.27	-6.24	18	1	-3395	-6.26	35	4	-3393.41	-6.48
4	5	-3392.16	-6.21	18	2	-3394.91	-6.27	35	5	-3393.4	-6.48
4	6	-3391.93	-6.18	18	3	-3394.9	-6.13	35	6	-3393.39	-6.68
4	7	-3390.71	-6.24	18	4	-3394.88	-6.13	35	7	-3388.28	-6.08
5	0	-3396.32	-6.67	19	0	-3395.18	-6.68	36	0	-3393.57	-5.97
5	1	-3396.31	-6.67	19	1	-3390.73	-6.27	36	1	-3393.55	-5.97
5	2	-3391.58	-6.25	20	0	-3395.18	-6.29	36	2	-3393.34	-6
5	3	-3391.57	-6.24	20	1	-3395.04	-6.26	36	3	-3393.3	-5.99
6	0	-3395.96	-6.54	21	0	-3395.08	-6.44	36	4	-3393.11	-5.97
6	1	-3395.93	-6.54	21	1	-3393.49	-6.46	36	5	-3392.26	-5.89
6	2	-3393.78	-6.31	21	2	-3393.36	-6.23	36	6	-3390.89	-5.76
6	3	-3391.95	-6.09	21	3	-3391.59	-6.3	36	7	-3390.55	-5.72
6	4	-3391.93	-6.09	21	4	-3391.25	-6.22	37	0	-3393.27	-6.27
6	5	-3390.95	-6.26	21	5	-3390.74	-6.32	38	0	-3393.19	-6.12
6	6	-3390.36	-5.86	21	6	-3390.68	-6.31	38	1	-3393.19	-6.12
6	7	-3390.2	-5.85	22	0	-3394.93	-6.24	38	2	-3391.84	-6.24
7	0	-3395.92	-6.4	22	1	-3394.93	-6.24	38	3	-3391.84	-6.24
7	1	-3395.89	-6.4	22	2	-3394.49	-6.17	39	0	-3392.79	-6.14
7	2	-3395.89	-6.4	22	3	-3394.49	-6.17	40	0	-3392.59	-6.45
7	3	-3395.83	-6.4	22	4	-3394.34	-6.17	40	1	-3392.44	-6.66
7	4	-3393.66	-6.41	22	5	-3394.32	-6.17	40	2	-3387.72	-6

7	5	-3393.66	-6.41	22	6	-3393.07	-6.07	40	3	-3386.28	-5.8
7	6	-3393.59	-6.42	22	7	-3393.03	-6.08	41	0	-3392.53	-5.98
7	7	-3391.93	-6.31	23	0	-3394.89	-6.84	41	1	-3392.52	-5.98
8	0	-3395.84	-6.29	23	1	-3390.83	-6.27	41	2	-3388.24	-5.84
8	1	-3393.91	-6.41	23	2	-3390.73	-6.54	42	0	-3391.63	-6.24
8	2	-3393.76	-6.33	23	3	-3389.9	-6.42	42	1	-3389.39	-5.82
8	3	-3393.31	-6.2	24	0	-3394.84	-6.2	43	0	-3391.1	-6.1
8	4	-3393.31	-6.2	24	1	-3394.79	-6.2	43	1	-3390.22	-6.11
8	5	-3392.97	-6.35	24	2	-3394.73	-6.2	44	0	-3391.1	-5.83
8	6	-3392.94	-6.34	24	3	-3392.8	-6.22	44	1	-3389.7	-5.98
9	0	-3395.68	-6.37	24	4	-3392.39	-6.19	44	2	-3389.7	-5.98
9	1	-3395.42	-6.24	24	5	-3392.39	-6.19	45	0	-3391.08	-5.79
9	2	-3395.34	-6.22	24	6	-3392.29	-5.95	46	0	-3391.02	-5.86
9	3	-3395.24	-6.27	24	7	-3392.24	-5.95	46	1	-3390.8	-5.88
10	0	-3395.6	-6.54	25	0	-3394.79	-6.25	47	0	-3390.72	-6
10	1	-3390.61	-6.06	26	0	-3394.73	-6.47	48	0	-3390.69	-5.92
11	0	-3395.57	-6.4	26	1	-3394.54	-6.1	48	1	-3387.04	-5.91
11	1	-3394.37	-6.25	26	2	-3392.48	-5.9	48	2	-3386.68	-5.51
11	2	-3394.36	-6.25	26	3	-3392.41	-6.06	48	3	-3386.63	-5.92
11	3	-3394.33	-6.24	26	4	-3392.38	-6.61	48	4	-3386.46	-5.89
11	4	-3392.79	-6.38	26	5	-3389.85	-5.85	49	0	-3390.4	-5.91
11	5	-3392.79	-6.38	27	0	-3394.71	-6.35	50	0	-3390.14	-6.74
11	6	-3392.51	-6.52	27	1	-3394.05	-6.3	51	0	-3389.65	-6.58
11	7	-3384.75	-5.78	27	2	-3393.49	-6.55	52	0	-3388.59	-5.95
12	0	-3395.4	-6.27	27	3	-3392.53	-6.19	53	0	-3388.33	-6.02
12	1	-3395.4	-6.27	27	4	-3389.68	-5.78	54	0	-3387.49	-6.34
12	2	-3395.4	-6.27	27	5	-3383.06	-6.05	55	0	-3387.43	-5.61

12	3	-3394.94	-6.14	27	6	-3378.14	-5.4	56	0	-3378.44	-5.8
12	4	-3394.93	-6.14	28	0	-3394.7	-6.28	56	0	-3378.44	-5.8
12	5	-3394.16	-6.15	28	1	-3393.07	-6.35				
12	6	-3394.02	-6.11	28	2	-3392.38	-6.31				
12	7	-3393.92	-6.11	28	3	-3390.89	-6.18				
13	0	-3395.35	-6.37	29	0	-3394.66	-6.2				
13	1	-3395.28	-6.36	29	1	-3394.26	-6.2				
13	2	-3395.21	-6.35	29	2	-3394.12	-6.21				
13	3	-3391.66	-6.15	29	3	-3394.07	-6.08				
13	4	-3388.34	-6.15	29	4	-3394.07	-6.08				
13	5	-3387.88	-5.93	29	5	-3393.93	-6.21				
13	6	-3387.4	-5.89	29	6	-3392.99	-6.07				



## **Chapter 02**

# **2,4'-Dihydroxybenzophenone exerts bone formation and anti-osteoporotic activity**

## Abstract

2,4'-Dihydroxybenzophenone (DHP) is an organic compound derived from *Garcinia xanthochymus*, but there are no reports on its biochemical functions and bioavailability. In this study, we evaluated whether DHP affects osteoblast differentiation and activation, as well as anti-osteoporotic activity in MC3T3-E1 preosteoblasts and zebrafish larvae. In the non-toxic concentrations, DHP-treated MC3T3-E1 preosteoblasts increased alkaline phosphatase (ALP) activation and mineralization in a concentration-dependent manner, accompanied by high expression of osteoblast-specific markers, including RUNX family transcription factor 2 (RUNX2), osterix (OSX), and ALP. Consistent with data in MC3T3-E1 preosteoblasts, DHP upregulated osteoblast-specific marker genes in zebrafish larvae and simultaneously stimulated vertebral formation. we also revealed that DHP enhanced phosphorylation of glycogen synthase kinase-3 $\beta$  (GSK-3 $\beta$ ) at SER9 and total expression of  $\beta$ -catenin in the cytosol, and markedly hastened localization of  $\beta$ -catenin into the nucleus. Furthermore, DHP restored prednisolone (PDS)-induced marked decrease in ALP activity and mineralization, as well as osteoblast-specific marker expression. In PDS-treated zebrafish, DHP alleviates PDS-induced osteoporosis in zebrafish larvae by restoring vertebral formation and osteoblast-specific gene expression. Taken together, these results suggest that DHP is a potential osteoanabolic candidate to treat osteoporosis by stimulating osteoblast differentiation.

**Key words:** DHP; Osteogenesis; Wnt/ $\beta$ -catenin; Osteoporosis

## 1. Introduction

Most individuals reach their peak bone mass at the age of 25 and 30, and thereafter, it gradually starts losing [1]. Although genetic factors play a significant role in determining peak bone mass across the lifespan, especially in the early life and early adulthood, environmental factors such as nutritional deficiency, diseases, and drugs severely affect functional capacities of bone in the elderly life rather than genetic factors [2]. In particular, osteoporosis is characterized by decreased bone mineral volume, and density accompanied by disruption of bone microarchitecture and is a major clinical problem in elderly men and women, especially postmenopausal [3]. Osteoporotic symptoms remain undiagnosed at the early stage and slowly hustle low trauma fracture of spine, hip, pelvis, proximal humerus, and wrist, which often results in hospitalization [4]. According to the International Osteoporosis Foundation, osteoporotic fractures is experienced by one in three women and one in five men over 50 years of age [5]. Osteoporosis is not only the leading cause of fractures in the elderly population, but also it is strongly linked to people becoming bedridden, which consequently reduces the quality of life [5]. Drug treatment using bisphosphonates, raloxifene, bazedoxifene, etc., is known as the best way to effectively reduce the risk of osteoporosis; however, not all drugs are available in every country, and long-term therapy is known in association with some side effects [6]. Therefore, dietary phytochemicals have been highlighted to improve bone mass and strength, and microarchitecture integrity, and translated into clinical studies [7].

Bone is a specialized connective tissue and consists of two types of tissue such as outer cortical bone (compact) which provides support and protection, and inner cancellous bone (spongy) which is less dense and biologically more active than the compact cortical bone [8]. To maintain bone homeostasis, three types of cells including osteoblasts, osteoclasts, and osteocytes collaboratively work under fine-tune control [9]. In particular, bone remodeling constantly undergoes through osteoclast-mediated bone resorption and osteoblast-mediated

bone formation [9, 10]. In this regard, for several decades, anti-resorptive drugs such as bisphosphonates, RANKL antibody, and selective estrogen receptor modulators, have been used for the treatment of osteoporosis, which stimulate osteoclast development, proliferation and activity and reduced vertebral fractures by approximately 50% and nonvertebral fractures by 20%, with some common side effects [11, 12]. Recently, anabolic drugs such as parathyroid hormone (PTH) receptor agonists—teriparatide and abaloparatide—directly activates osteoblast differentiation and function, as synthesis of bone matrix, leading to bone formation [13-15]. Although it is unknown whether it is due to an exact causal relationship in human, Vahle et al. reported that long-term medication of PTH receptor agonists increased risk factors such as osteosarcoma in rats [16] and failure between bone formation and resorption for a period time [17]. In this regard, for a long, plant-derived compounds such as polyphenols have been considered excellent candidates to stimulate bone anabolism targeting osteoblast maturation and activation [18, 19].

Wingless-related integration site (Wnt)/ $\beta$ -catenin signaling pathway is specifically important for osteoblast differentiation, bone formation, and treatment of bone diseases, such as osteoporosis [20]. In the canonical Wnt signaling pathway, the Wnt1 class ligands binds to low-density lipoprotein receptor-related proteins 5 or 6 (LRP5/6) and frizzled (FzD) receptor, and recruits Disheveled (DSH) to bind a destruction complex including glycogen synthase kinase-3 $\beta$  (GSK-3 $\beta$ ) and Axin, leading to release  $\beta$ -catenin from the complex [21]. Accumulated  $\beta$ -catenin translocate in the nucleus and propels the transcriptional corepressor Grouch from T cell factor/lymphoid enhancer binding factor (TcF/LeF), resulting in transactivation of genes, including related Runt-related transcription factor 2 (RUNX2) and osterix (OSX), to osteoblast differentiation and maturation [22, 23]. During osteogenesis, two master genes, RUNX2 and OSX, turn on at a different period of times; RUNX2 promotes differentiation from bone marrow mesenchymal stem cell to preosteoblast, and OSX positively

regulates osteoblast differentiation at the late stage [24, 25]. In recent, many natural products are promising candidates to stimulate osteoblast maturation and bone formation by activation the canonical Wnt/ $\beta$ -catenin signaling pathway, leading to protection of osteoporosis [26-28].

Benzophenone and its derivatives are organic compound and have been used as ultraviolet curing agents, especially, cosmetics that prevent UV-induced damage [29]. Nevertheless, some derivatives, including benzophenone-3 and octocrylene, affect toxicity in algae, corals, fish, and mammals through heavy accumulation in the environment [30]. In the other hand, some benzophenone derivatives from plants and marine fungus showed anticancer activity through inhibiting human p-glycoprotein [31], the NF- $\kappa$ B signaling pathway [32], and the MEK/ERK pathway [33]. Recently, Arshia et al. demonstrated that benzophenone thio/semicarbazone derivatives show potential anti-glycemic activity by directly inhibiting [34]. However, studies on various biochemical and physiological activity mechanisms of the derivatives are still insufficient. In this study, we evaluated whether 2,4'-dihydroxybenzophenone (DHP) derived from the herb, *Garcinia xanthochymus* affects bone formation and anti-osteoporosis in mouse MC3T3E1 preosteoblasts and zebrafish larvae.

## 2. Materials and methods

### 2.1. Regents and antibodies

DHP was purchased from ChemFaces (Fig. 1.1, Wuhan, Hubei, China). Trypsin-ethylenediaminetetraacetic acid solution, fetal bovine serum (FBS), antibiotic mixture, and  $\alpha$ -Modification of Minimum Essential Medium ( $\alpha$ -MEM) were obtained from WELGENE (Gyeongsan-si, Gyeongsangbuk-do, Republic of Korea). Alizarin red, calcein, 2,5-diphenyltetrazolium bromide (MTT),  $\beta$ -glycerophosphate (GP), and prednisolone (PDS) were purchased from Sigma Aldrich (St. Louis, MO, USA). Antibodies against RUNX2 (sc-101145), OSX (sc-393325), ALP (sc-398461),  $\beta$ -actin (sc-69879), GSK-3 $\beta$  (sc-814662), phosphor (p)-GSK-3 $\beta$  at SER9 (sc-37800)  $\beta$ -catenin (sc-59737), and nucleolin (C23, sc-13057) were obtained from Santa Cruz Biotechnology (Dallas, TX, USA). Peroxidase-labeled anti-rabbit immunoglobulins (KO211708) and peroxidase-labeled anti-mouse immunoglobulins were purchased from Koma Biotech (Seoul, Republic of Korea) and Santa Cruz Biotechnology, respectively. All other chemicals were purchased from Sigma-Aldrich.

### 2.2. Cell culture and MTT assay

The mouse MC3T3-E1 preosteoblast cells were obtained from American Type Culture Collection (Manassas, VA, USA) and cultured in  $\alpha$ -MEM supplemented with 10% FBS and antibiotic mixture at 37°C in a humidified incubator at 5% of CO<sub>2</sub>. MC3T3-E1 cells ( $1 \times 10^4$  cells/ mL) were treated with DHP (0–100  $\mu$ M) for 14 days to evaluate cell viability. The media with DHP was replaced every 2 days. On day 14, MTT (0.5 mg/ml) solution was treated in the cells for 4 h, and dimethyl sulfoxide (DMSO) was used to dissolve the formazan. Absorbance was measured at 570 nm using a microplate reader (Thermo Fisher Scientific, Rockford, IL, USA). In a separate experiment, phase-contrast microscopy (Macrotech, Goyang-si, Gyeonggi-do, Republic of Korea) was used to examine cell morphology.

### 2.3. Flow cytometry analysis

MC3T3-E1 cells ( $1 \times 10^4$  cells/mL) were treated with DHP (0–100  $\mu$ M) for 14 days, and the media were replaced with the indicated concentrations of DHP (0–100  $\mu$ M) every 2 days. Viable cell count and dead cell population were examined on day 14. Briefly, harvested cells were washed with phosphate-buffered saline (PBS) and stained for 5 min using a Muse Cell Count & Viability Kit (Luminex, Austin, TX, USA). Then, the stained cells were analyzed using Muse Cell Analyzer (Luminex).

### 2.4. Alkaline phosphatase (ALP) and alizarin red staining

MC3T3-E1 cells ( $1 \times 10^4$  cells/ml) were treated with the indicated concentrations of DHP (0–10  $\mu$ M) or GP (2 mM) for 14 days. In a parallel study, 10  $\mu$ M PDS was treated 2 h before exposure to DHP for 14 days. Cell culture media were replaced every 2 days with the indicated chemicals. For the ALP staining, a Tartrate-resistant Acid Phosphatase (TRACP) and Alkaline Phosphatase (ALP) Double-staining Kit (Takara Bio, Kusatsu, Shiga, Japan) was used following the manufacturer's protocol. In brief, cells were washed with PBS and fixed for 5 min using the fixation solution provided. Then, the ALP substrate was added to the cells and incubated at 37°C for 45 min. For alizarin red staining (mineralization), cells were washed with PBS and fixed with 4% paraformaldehyde at 37°C for 10 min. Then, the cells were washed with distilled water and stained with 2% alizarin red solution. Representative images were captured using phase-contrast microscopy (Macrotech).

### 2.5. Isolation of mRNA from MC3T3-E1 cells and reverse transcription-polymerase chain reaction (RT-PCR)

Under the same condition as mentioned in 2.4., total RNA was extracted from MC3T3-E1 cells using an easy-BLUE Total RNA Extraction Kit (iNtRON Biotechnology, Seongnam, Gyeonggi-do, Republic of Korea) on day 14. Reverse transcription was performed using MMLV reverse transcriptase (Bioneer, Daejeon-si, Republic of Korea), and cDNA was

amplified using EzWay Neo Taq PCR MasterMix (Koma Biotech). The specific primers used in this study were shown in Table 3. The expressional value was normalized to the intensity level of glyceraldehyde-3-phosphate dehydrogenase (GAPDH).

Table 3: Primer sequences used in this study.

Species	Gene	Primer sequence (5' -3')	Size (bp)	Accession no.
mouse	<i>OSX</i>	F: 5'-AAGGCGGTTGGCAATAGTGG-3'	195	NM 130458.4
		R: 5'-GCAGCTGTGAATGGGCTTCT-3'		
	<i>RUNX2</i>	F: 5'-CATGGTGGAGATCATCGCGG-3'	172	NM 001146038.2
		R: 5'-GGCCATGACGGTAACCACAG-3'		
<i>ALP</i>	F: 5'-TTGTGGCCCTCTCCAAGACA-3'	199	NM 007431.3	
	R: 5'-GACTTCCCAGCATCCTTGGC-3'			
<i>GAPDH</i>	F: 5'-ACCACAGTCCATGCCATCAC-3'	450	NM 001289726.2	
	R: 5'-CACCACCCTGTTGCTGTAGC-3'			
zebrafish	<i>OSX</i>	F: 5'-GGCTATGCTAACTGCGACCTG-3'	154	NM 212863.2
		R: 5'-GCTTTCATTGCGTCCGTTTT-3'		
	<i>RUNX2a</i>	F: 5'-GACGGTGGTGACGGTAATGG-3'	174	NM 212858.2
		R: 5'-TGCGGTGGGTTCGTGAATA-3'		
	<i>ALP</i>	F: 5'-CAAGAACTCAACAAGAAC-3'	149	NM 201007.2
		R: 5'-TGAGCATTGGTGTTATAC-3'		
	<i>β-actin</i>	F: 5'-CGAGCGTGGCTACAGCTTCA-3'	155	NM 131031.2
		R: 5'-GACCGTCAGGCAGCTCATAG-3'		

## 2.6. Western blotting

Under the same condition as mentioned in 2.4. and 2.9., total cellular protein was prepared using RIPA Lysis Buffer (iNtRON Biotechnology) with protease inhibitors (Sigma-Aldrich). Nuclear protein was extracted using an NE-PER Nuclear and Cytoplasmic Extraction Reagents (Thermo Fisher Scientific). A Bio-Rad Protein Assay Kit (Bio-Rad Laboratories, Hercules, CA,



USA) was used for quantifying protein concentrations. Equal amount of proteins (30  $\mu\text{g}$ ) was immediately used for western blotting or stored at  $-80^{\circ}\text{C}$ . Then, the proteins were separated on sodium dodecyl sulfate-polyacrylamide gels and transferred to a nitrocellulose membrane (Thermo Fisher Scientific). Using the primary (200  $\mu\text{g}/\text{mL}$ , 1:1000 dilution) and secondary (400  $\mu\text{g}/\text{mL}$ , 1:3,000 dilution) antibodies, immunoblotting was performed, and bound antibodies were detected using a SuperSignal West Pico PLUS Kit (Thermo Fisher Scientific). Images were captured using ImageQuant LAS 500 (GE Healthcare Bio-Sciences AB, Uppsala, Sweden). The expressional value was normalized to the intensity level of  $\beta$ -actin or nucleolin.

### 2.7. Zebrafish maintenance

Zebrafish were raised according to the relevant regulations and guidelines given by the Animal Care and Use Committee of Jeju National University (Jeju Special Self-governing province, Republic of Korea; (approval No: 2022-0085), and the methods were conducted according to the approved guidelines [35]. Embryos were collected using natural spawning and cultured in embryo medium (34.8 g NaCl, 1.6 g KCl, 5.8 g  $\text{CaCl}_2 \cdot 2\text{H}_2\text{O}$ , 9.78 g  $\text{MgCl}_2 \cdot 6\text{H}_2\text{O}$  in 1 L double-distilled water, pH 7.2) supplemented with 1% methylene blue at  $28^{\circ}\text{C}$ .

### 2.8. Vertebral formation in zebrafish larvae

Calcein staining was used to evaluate the vertebral formation in zebrafish larvae as previously described [26-28]. Briefly, zebrafish larvae at 3 days post fertilization (dpf,  $n=20$ ) were treated with the indicated concentrations of DHP (0–10  $\mu\text{M}$ ) or 4 mM GP until 9 dpf. In a parallel experiment, 10  $\mu\text{M}$  PDS was treated in 5 dpf zebrafish larvae 2 h before DHP treatment until 9 dpf. The embryo medium and the chemicals were replaced every 2 days. At 9 dpf, larvae were immersed in 1% calcein solution for 10 mins and anesthetized in 0.04% tricaine methanesulfonate solution. Then, fluorescence images were captured using a CELENA S Digital Imaging System (LogosBiosystems, Anyang, Gyeonggi-do, Republic of Korea).

### 2.9. Isolation of mRNA from zebrafish larvae and RT-PCR

Under the same condition as mentioned in 2.8., total RNA was extracted from zebrafish larvae at 9 dpf using an easy-BLUE Total RNA Extraction Kit (iNtRON Biotechnology, Seongnam, Gyeonggi-do, Republic of Korea). MMLV reverse transcriptase (Bioneer) and EzWay Neo Taq PCR MasterMix (Koma Biotech) were used for reverse transcription and cDNA amplification, respectively. The specific primers used in this study were shown in Table 1. The expressional value was normalized to the intensity level of  $\beta$ -actin.

### 2.10. Statistical analysis

ImageJ (National Institute of Health, Bethesda, MD, USA) was used to quantify gene and protein expression. The data were fit using a modified three-parameter exponential decay using SigmaPlot Version 12.5 (Systat Software, San Jose, CA, USA, [www.systatsoftware.com](http://www.systatsoftware.com)). Student's t-test or one-way ANOVA with Bonferroni correction was used to determine significant differences among each group. Values were presented as the standard error of the mean (SEM). \*\*\* and ###  $p < 0.001$ , and \*\*  $p < 0.05$ , were considered to indicate statistical significance.

### 3. Results

#### 3.1. DHP at a concentration of 100 $\mu$ M is cytotoxic to MC3T3-E1 preosteoblast cells

To evaluate the effect of DHP on MC3T3E-1 cell viability, MTT assay, morphological analysis, and flow cytometry were performed. No cytotoxicity was observed at DHP concentration below 10  $\mu$ M on day 14, DHP concentration of 100  $\mu$ M significantly decreased relative cell viability to  $57.0 \pm 0.5\%$  (Fig. 2.1A). Additionally, low concentrations of DHP (0–10  $\mu$ M) did not induce any morphological changes; however, 100  $\mu$ M DHP treatment resulted in remarkably reduced cell population and floating cells (Fig. 2.1B). As shown in Fig. 2.1C, flow cytometric analysis further confirmed that a high concentration of DHP (100  $\mu$ M) decreased the viable cell count ( $0.3 \times 10^5$  cells/mL, Fig. 2.1D) and increased dead cell population ( $33.2 \pm 1.8\%$ , Fig. 2.1E) compared to those of the untreated cells ( $3.0 \times 10^5$  cells/mL and  $8.8 \pm 0.7\%$  respectively). Consistent with relative cell viability, no changes in viable cell count and dead cell population were shown at low concentrations. These results indicate that low concentrations of DHP are not cytotoxic to MC3T3-E1 preosteoblast cells until day 14.

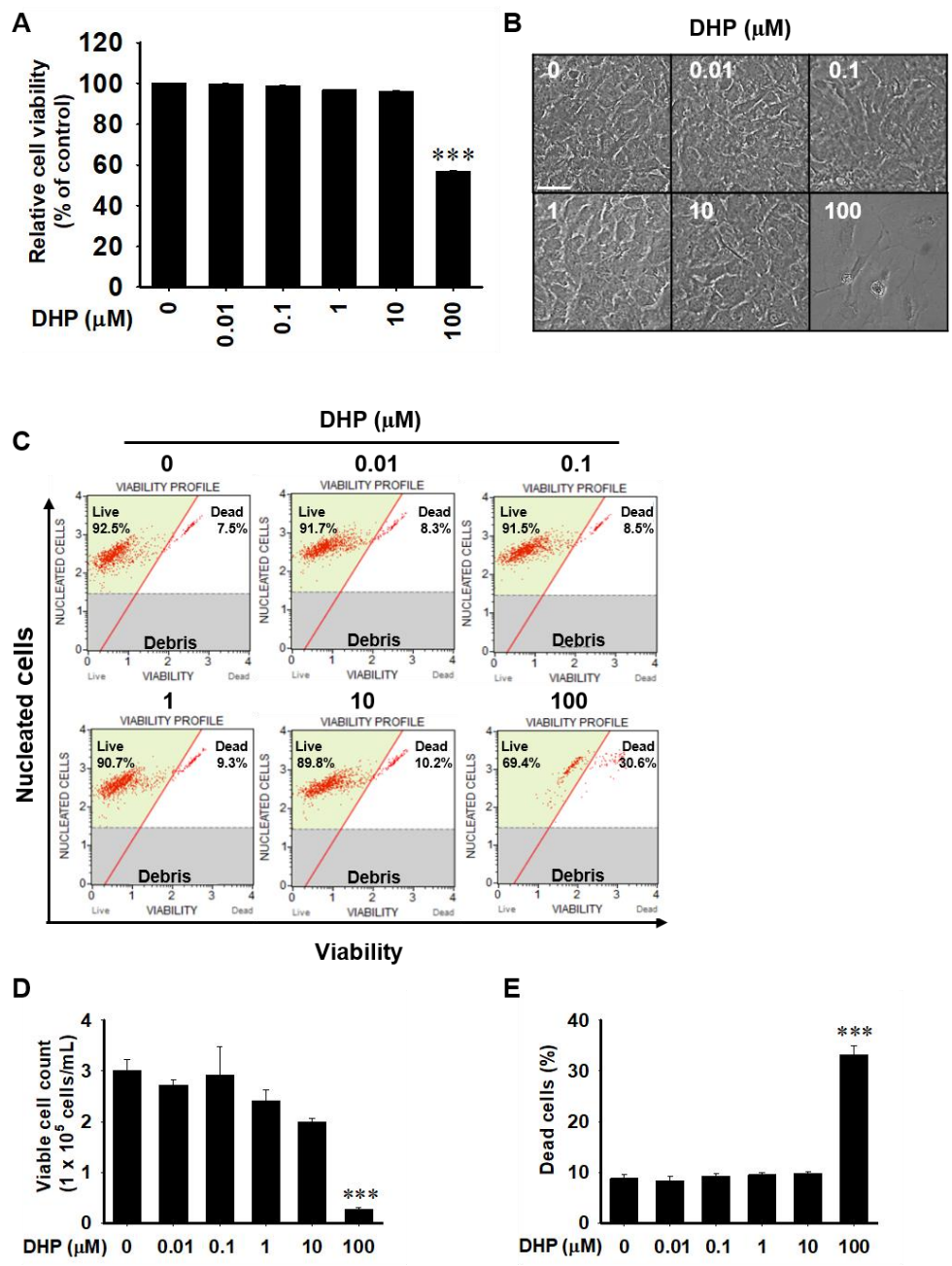


**Fig. 2.1.** DHP at a concentration of 100  $\mu\text{M}$  decreases viability of MC3T3-E1 preosteoblasts. MC3T3-E1 preosteoblast ( $1 \times 10^4$  cells/mL) were treated with DHP (0–100  $\mu\text{M}$ ) for 14 days. The media were replaced every 2 days. (A) Relative cell viability was determined using an MTT assay. (B) Morphological changes in MC3T3-E1 preosteoblasts were monitored using stereomicroscopy. Scale bar = 50  $\mu\text{m}$  (C) Viability in the nucleated cells was measured using flow cytometry. (D) Viable cell count and (E) dead cell population were obtained from flow

cytometric analyses. Data are represented as the mean  $\pm$  SEM of three independent experiments ( $n=3$ ). \*\*\*,  $p < 0.001$  vs. untreated cells.

### 3.2. DHP promotes osteoblast differentiation in MC3T3-E1 preosteoblast cells

To evaluate the osteogenic ability of DHP, MC3T3-E1 preosteoblast cells were treated with the indicated concentrations of DHP (0–10  $\mu$ M) for 14 days. ALP activity (Fig. 2.2A) and alizarin red staining (Fig. 2.2B) indicate that DHP induces the formation of new bone and mineralization in a concentration-dependent manner. The highest concentration of DHP (10  $\mu$ M) significantly increased the osteogenic potentials including ALP activity and mineralization on day 14, comparable to the cells treated with GP. Furthermore, DHP treatment concentration-dependently increased the expression of osteoblast-specific genes, including *RUNX2*, *OSX*, and *ALP* on day 14 (Fig. 2.2C). The highest concentration of DHP significantly increased the osteoblast-specific gene expressions commensurate with GP-treated cells. Moreover, as with the results of gene expression, DHP treatment increased the expression of osteoblast-specific proteins, including *RUNX2*, *OSX*, and *ALP* on day 14 in a concentration-dependent manner (Fig. 2.2D). These results indicate that DHP promotes osteoblast differentiation and maturation in accordance with expression of genes and proteins related to osteoblast differentiation and maturation.

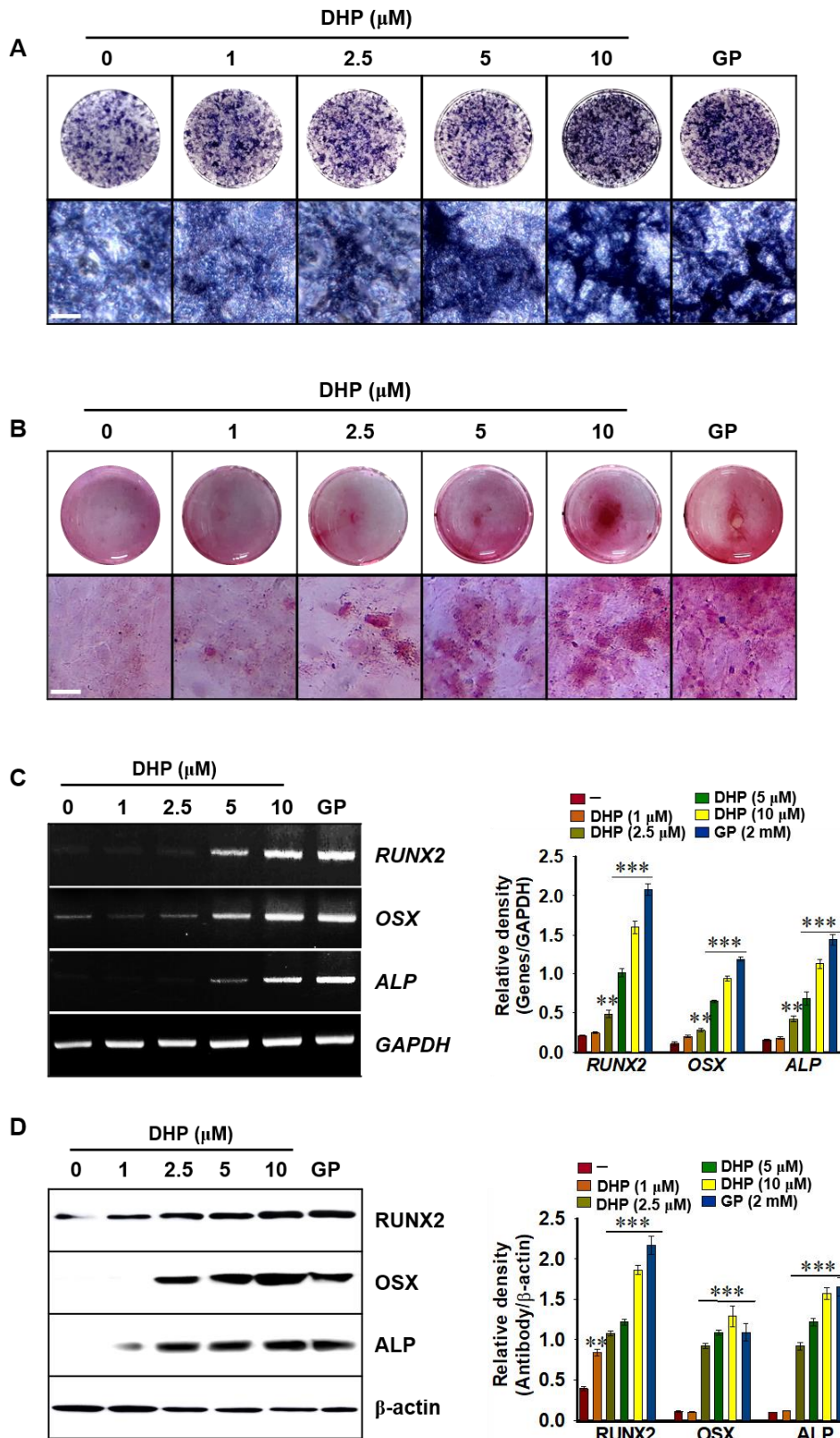


**Fig. 2.2.** DHP stimulates osteoblast differentiation. MC3T3-E1 preosteoblasts ( $1 \times 10^4$  cells/mL) were treated with DHP (0–10  $\mu\text{M}$ ) for 14 days.  $\beta$ -Glycerophosphate (GP, 2 mM) was used as the positive control. The media were replaced every 2 days with the indicated chemicals. (A)

The cells were stained using a TRACP and ALP Double-Staining Kit and (B) 2% alizarin red solution. Representative images were captured using phase-contrast microscopy ( $\times 10$ ). Scale bar = 50  $\mu\text{m}$ . (C) Total mRNA was extracted on day 14, and RT-PCR was performed to detect the expression of *RUNX2*, *OSX*, and *ALP*. Glyceraldehyde-3-phosphate dehydrogenase (*GAPDH*) was used as the loading control. (D) Total protein was isolated on day 14, and western blotting was performed to detect the expression of osteoblast marker proteins, including *RUNX2*, *OSX*, and *ALP*.  $\beta$ -Actin was used as the loading control. The relative density was calculated using ImageJ software and normalized to the intensity of *GAPDH* and  $\beta$ -Actin. \*\*\*,  $p < 0.001$  and \*\*,  $p < 0.01$  vs. untreated cells.



### 3.3. DHP enhances vertebral formation in zebrafish larvae

Calcein staining was performed to investigate whether DHP promotes vertebral formation in zebrafish larvae. Zebrafish larvae at 3 dpf were treated with DHP (0–10  $\mu$ M) until 9 dpf, and calcein staining was performed. Our results indicate that DHP increases vertebral formation in 9 dpf zebrafish larvae in a concentration-dependent manner (Fig. 2.3A) and the total vertebrae number was increased in a concentration-dependent manner ( $6.4 \pm 0.3$ ,  $7.6 \pm 0.3$ ,  $7.7 \pm 0.3$ , and  $9.2 \pm 0.2$  at 1, 2.5, 5, and 10  $\mu$ M DHP, respectively) compared to that of the untreated zebrafish larvae ( $5.5 \pm 0.3$ , Fig. 2.3B). Additionally, GP treatment dramatically increased the vertebrae formation compared to that of the control group ( $11.2 \pm 0.3$ , Fig. 2.3B). Furthermore, relative bone intensity in 9 dpf zebrafish larvae was increased with DHP treatment in a concentration-dependent manner ( $123.8 \pm 7.3$ ,  $188.7 \pm 14.9$ ,  $225.3 \pm 6.5$ ,  $255.3 \pm 6.7$  at 1, 2.5, 5 and 10  $\mu$ M DHP, respectively) compared to that of the untreated zebrafish larvae ( $100.0 \pm 4.4$ , Fig. 2.3C). The bone intensity in GP-treated zebrafish larvae was comparatively higher ( $297.1 \pm 6.3$ ) than 10  $\mu$ M DHP treatment. Osteoblast-specific gene expression, including *RUNX2a*, *OSX*, and *ALP* were significantly upregulated in zebrafish larvae treated with DHP or GP (Fig. 2.3D). These results suggest that DHP stimulates bone formation in zebrafish larvae by upregulating osteoblast-specific gene expression.

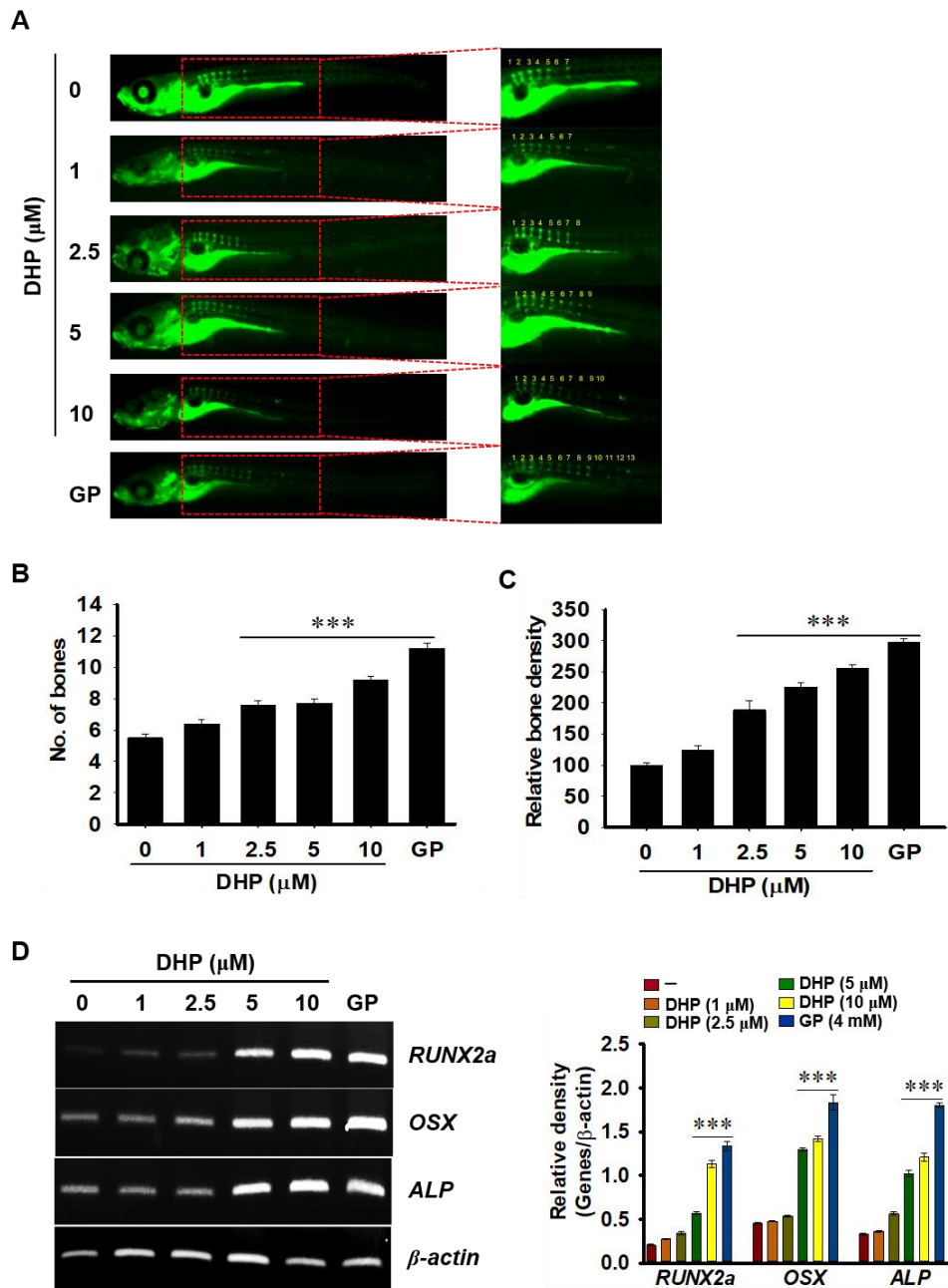


**Fig. 2.3.** DHP promotes vertebral formation in zebrafish larvae. The indicated concentrations of DHP (0–10  $\mu\text{M}$ ) were treated to 3 dpf zebrafish larvae and raised up to 9 dpf.  $\beta$ -Glycerophosphate (GP, 4 mM) was used as the positive control. The media were replaced with the indicated chemicals every 2 days. (A) At 9 dpf, zebrafish larvae were stained with 1% calcein solution to visualize vertebral formation. (B) The number of vertebrae was manually counted. (C) Bone density was measured by ImageJ software and normalized to that of untreated zebrafish larvae. (D) In a parallel experiment, total mRNA was extracted, and RT-

PCR was performed to detect the expression of *RUNX2a*, *OSX*, and *ALP*.  $\beta$ -Actin was used as the loading control. The relative density was calculated using ImageJ software and normalized to the density of  $\beta$ -actin. \*\*\*,  $p < 0.001$  vs. untreated zebrafish larvae.

### *3.4. DHP upregulates GSK-3 $\beta$ phosphorylation and subsequent $\beta$ -catenin activation*

To investigate whether DHP induces osteoblast differentiation by activating the canonical Wnt/ $\beta$ -catenin pathway, we examined expression of GSK-3 $\beta$  and  $\beta$ -catenin. As shown in Fig. 2.4A, DHP upregulated phosphorylated GSK-3 $\beta$  (at SER9) and  $\beta$ -catenin expression in total proteins extracted from MC3T3-E1 cells in a concentration-dependent manner. GP used as a positive control for bone formation markedly increased those expressions as much as similar to treatment with 10  $\mu$ M DHP. Additionally, we evaluated nuclear translocation of  $\beta$ -catenin, because phosphorylation of GSK-3 $\beta$  at SER9 releases  $\beta$ -catenin from a destructive complex and free  $\beta$ -catenin translocates to nucleus and consequently transactivates osteoblast-specific gene expression [21-23]. Our western blotting results indicated that nuclear translocation of  $\beta$ -catenin is also upregulated by DHP in a concentration-dependent manner (Fig. 2.4B). Therefore, these results indicate that DHP promotes nuclear translocation of  $\beta$ -catenin through the phosphorylation of GSK-3 $\beta$  at SER9 in MC3T3-E1 cells.

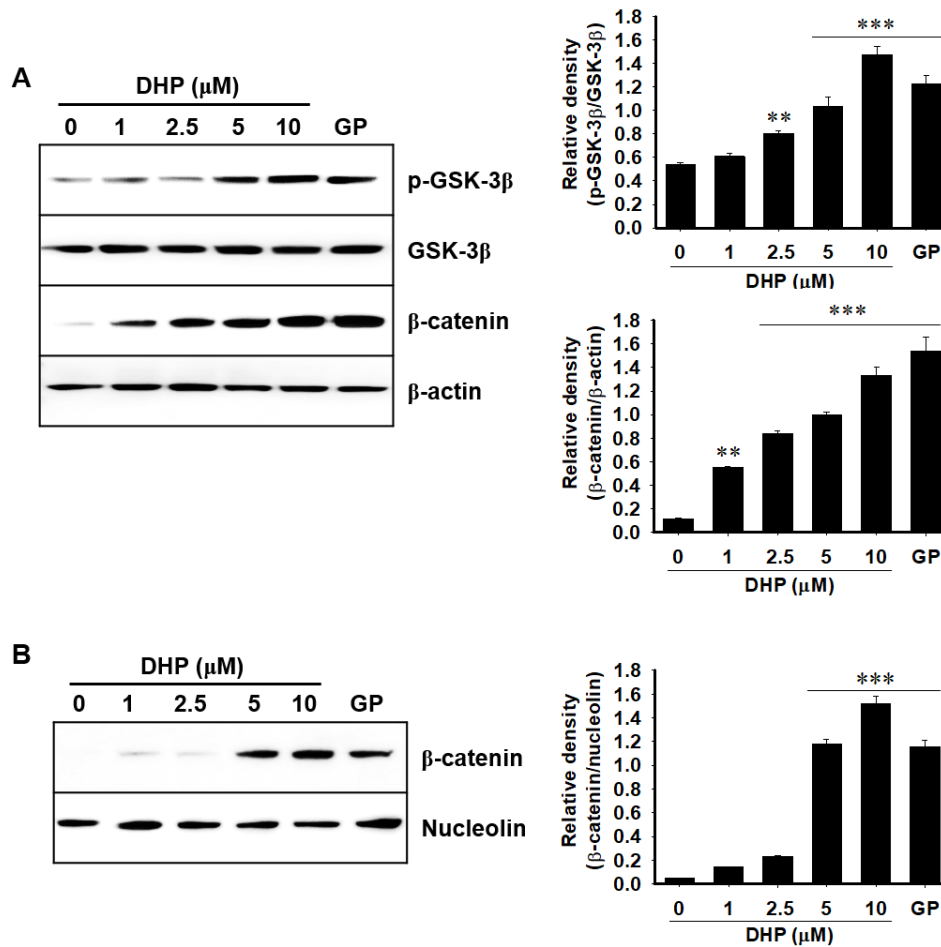


**Fig. 2.4.** DHP promotes GSK-3β phosphorylation at SER9 and subsequent β-catenin activation. MC3T3-E1 preosteoblasts ( $1 \times 10^4$  cells/mL) were cultured with indicated concentrations of DHP for 14 days. β-Glycerophosphate (GP, 2 mM) was used as the positive control. The media were replaced every 2 days. (A) Total proteins were extracted, and western blotting was performed to detect the expression of phospho (p)-GSK-3β at SER9, GSK-3β, and β-catenin. β-Actin was used as the loading control. (B) Nuclear proteins were extracted, and western blotting was performed to detect the expression of β-catenin. Nucleolin was used as the loading control. The relative density was calculated using ImageJ software and normalized to the density of β-actin and β-catenin, respectively. \*\*\*,  $p < 0.001$  and \*\*,  $p < 0.01$  vs. untreated cells.

### 3.5. DHP abates PDS-induced anti-osteogenic properties in MC3T3E-1 cells

To investigate whether DHP ameliorates PDS-induced impaired osteoblast differentiation and mineralization, MC3T3-E1 cells were treated with the indicated concentrations of DHP in the presence or absence of PDS for 14 days. As expected, PDS treatment significantly decreased ALP activity (Fig. 2.5A) and calcification (Fig. 2.5B) on day 14. However, DHP markedly restored ALP activity and mineralization reduced by PDS treatment. In a parallel study, we observed that PDS dramatically downregulated osteoblast-specific gene expression, including *RUNX2*, *OSX*, and *ALP*. However, DHP revitalized the osteoblast-specific gene expressions in the presence of PDS (Fig. 2.5C). Furthermore, we investigated whether DHP affects the protein expression related to osteoblast differentiation altered by PDS. Consistent with the data on osteoblast-specific gene expression, western blotting results indicated that DHP recovered PDS-induced reduction of the proteins, including *RUNX2*, *OSX*, and *ALP* in MC3T3-E1 cells in a concentration-dependent manner. Therefore, these results suggest that DHP alleviates PDS-induced anti-osteogenic properties in MC3T3-E1 cells.

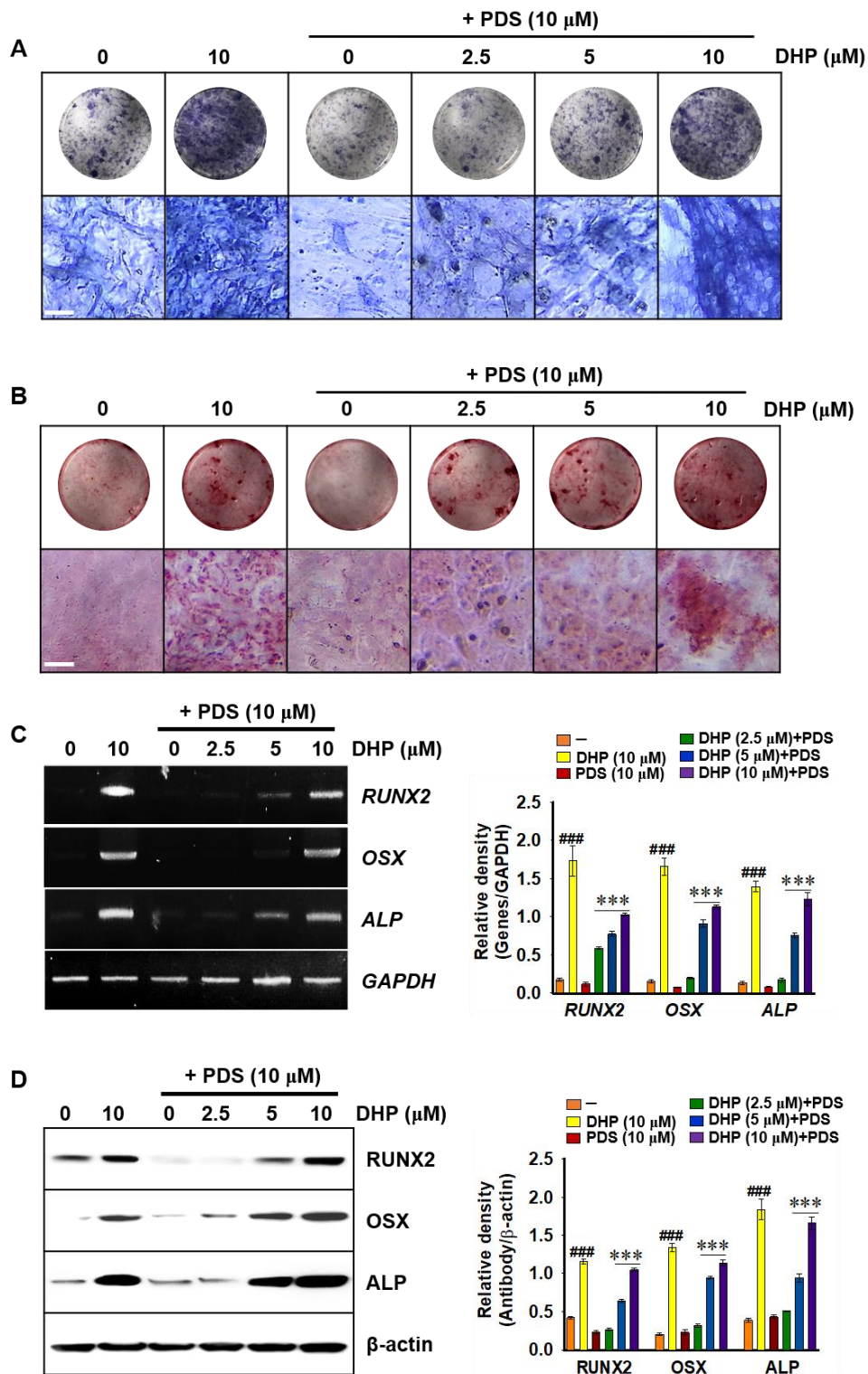


**Fig. 2.5.** DHP restored osteoblast differentiation impaired by prednisolone (PDS). MC3T3-E1 preosteoblasts ( $1 \times 10^4$  cells/mL) were treated with DHP (0–10  $\mu$ M) for 14 days in the presence of PDS (10  $\mu$ M). The media were replaced with the indicated chemicals every 2 days. (A) Cells were stained using a TRACP and ALP Double-Staining Kit and (B) 2% alizarin red solution.

Representative images were captured using phase-contrast microscopy ( $\times 10$ ). Scale bar = 50  $\mu\text{m}$ . (C) Total RNA was extracted on day 14, and RT-PCR was performed to detect the expression of *RUNX2*, *OSX*, and *ALP*. Glyceraldehyde-3-phosphate dehydrogenase (*GAPDH*) was used as the loading control. (D) Total protein was isolated, and western blotting was performed to detect the expression of osteoblast marker proteins, including *RUNX2*, *OSX*, and *ALP*.  $\beta$ -Actin was used as the loading control. The relative density was calculated using ImageJ software and normalized to the density of *GAPDH* and  $\beta$ -Actin, respectively. ###,  $p < 0.001$  vs. untreated cells and \*\*\*,  $p < 0.001$  vs. PDS-treated cells.



### 3.6. DHP alleviates PDS-induced osteoporosis in zebrafish larvae

To investigate whether DHP alleviates PDS-induced osteoporosis in zebrafish larvae, PDS was treated in 5 dpf zebrafish larvae 2 h before DHP treatment until 9 dpf, and calcein staining was performed (Fig. 2.6A). As we expected, PDS treatment dramatically reduced the vertebral number at 9 dpf ( $3.5 \pm 0.3$ ) compared to that of the untreated zebrafish larvae ( $6.0 \pm 0.3$ ). However, DHP restored the reduced bone number of PDS-treated zebrafish larvae to  $5.0 \pm 0.2$ , and  $6.2 \pm 0.3$  at 5 and 10  $\mu\text{M}$ , respectively (Fig. 2.6B). DHP at a concentration of 2.5  $\mu\text{M}$  did not recover the vertebral number in the presence of PDS. Furthermore, we identified that relative vertebral intensity in PDS-treated zebrafish larvae was significantly decreased ( $49.0 \pm 1.8$ ) compared to that of the untreated zebrafish larvae ( $100.0 \pm 4.7$ ). However, DHP treatment restore the reduced vertebral density in PDS-treated zebrafish larvae to  $107.6 \pm 10.2$  and  $139.6 \pm 4.7$  at 5 and 10  $\mu\text{M}$ , respectively (Fig. 2.6C). Consistent with data of Fig. 7B, no discrete vertebral recovery in PDS-treated zebrafish larvae was observed at the lowest concentration of DHP (2.5  $\mu\text{M}$ ,  $59.0 \pm 2.5$ ). Additionally, expression of osteoblast-specific genes, including *RUNX2a*, *OSX*, and *ALP* were strongly downregulated in PDS-treated zebrafish larvae (Fig. 2.6D). However, DHP strongly recuperated the impaired gene expression in PDS-treated zebrafish larvae in a concentration-dependent manner. These results suggest that DHP alleviates PDS-induced osteoporosis in zebrafish larvae by restoring the osteoblast-specific gene expression.

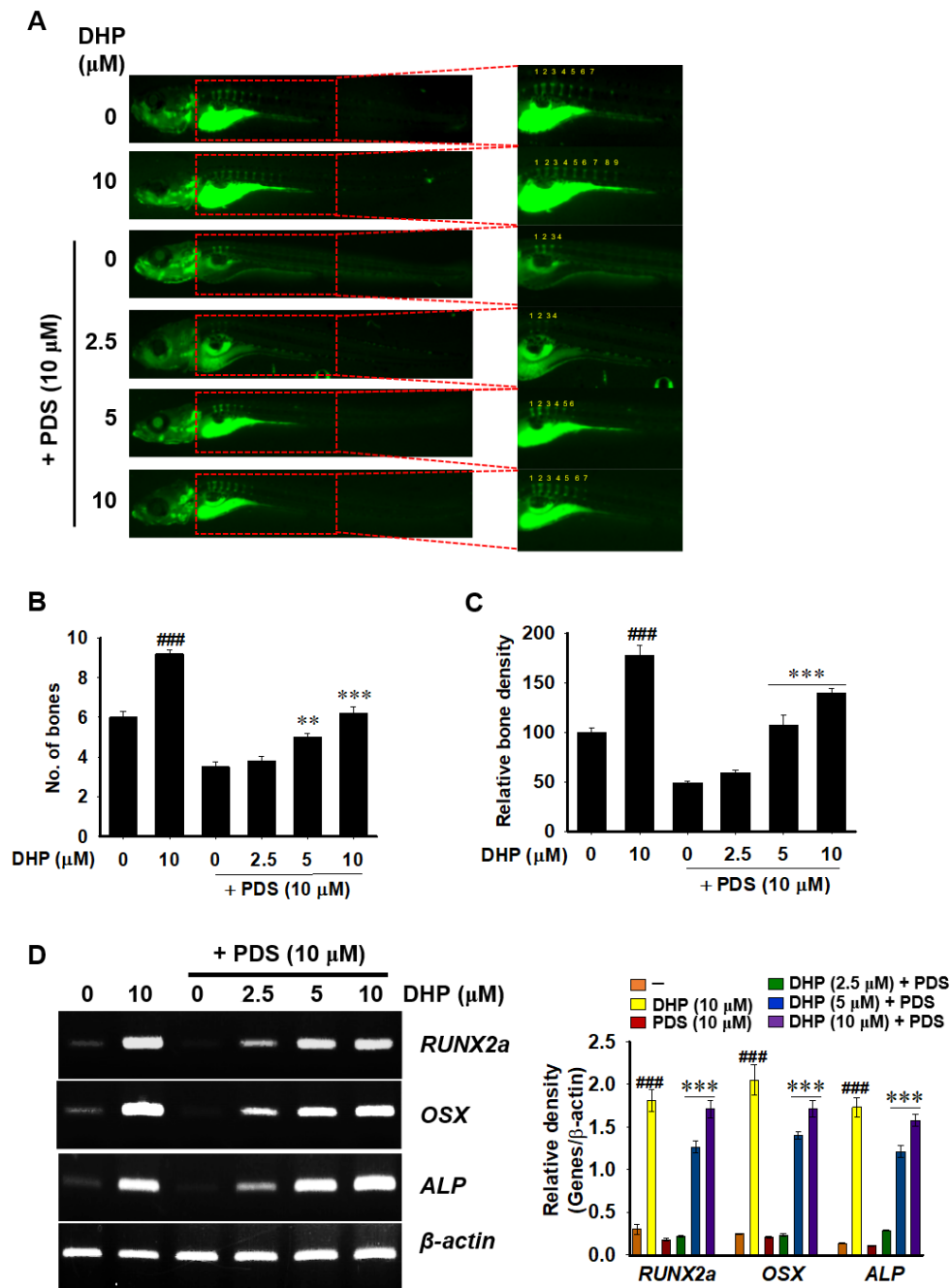


**Fig. 2.6.** DHP recovers prednisolone (PDS)-induced impaired vertebral formation. Zebrafish larvae at 5 dpf ( $n=20$ ) were treated with PDS ( $10 \mu\text{M}$ ) 2 h before DHP treatment ( $0\text{--}10 \mu\text{M}$ ) until 9 dpf. (A) At 9 dpf, zebrafish larvae were stained with 1% calcein solution to visualize vertebral formation. (B) The number of vertebrae was manually counted and numbered (yellow). (C) Bone density was measured using ImageJ software and normalized to that of untreated zebrafish larvae. (D) In a parallel experiment, total RNA was extracted, and RT-PCR was performed to detect the expression of *RUNX2a*, *OSX*, and *ALP*.  $\beta$ -Actin was used as the loading

control. The relative density was calculated using ImageJ software and normalized to the density of  $\beta$ -Actin. ###,  $p < 0.001$  vs. untreated zebrafish larvae, and \*\*\*,  $p < 0.001$  and \*\*,  $p < 0.01$  vs. PDS-treated zebrafish larvae.

#### 4. Discussion

As the incidence of osteoporosis increases, especially in the elderly, it has emerged as a global social and health issue accompanied by economic problem [36]. Antiresorptive agents, including bisphosphonates, nuclear factor kappa B (NF- $\kappa$ B) ligand-activated receptor (RANKL) inhibitors, and glucocorticoids have been commonly used as treatment option of osteoporosis by inhibiting osteoclast activity and thereby reducing bone resorption [37]. However, long-term medication of bisphosphonates or a RANKL inhibitor, denosumab, is associated with increased bone brittleness and excessive inhibition of bone resorption, which leads to mandibular osteonecrosis [38]. Prolonged glucocorticoid medication also results in increased apoptosis and impaired osteoblast differentiation and leads to glucocorticoid-induced osteoporosis [39]. Recently, anabolic agents directly targeting osteoblast maturation and new bone formation, are considered to be superior to antiresorptive agents in the treatment of osteoporosis; however, they still possess mild side effects, such as headache and nausea [40]. Hence, naturally plant-derived compounds such as polyphenols have been underlined to treat osteoporosis as emerging osteoanabolic agents [18, 19]. In this study, we investigated the osteoanabolic and anti-osteoporotic effects of DHP derived from the herbs of *Garcinia xanthochymus*, which had not been reported so far. We found that DHP stimulates differentiation, maturation, and mineralization of MC3T3-E1 preosteoblast cells and increases vertebral formation in zebrafish larvae by activating the canonical Wnt/ $\beta$ -catenin signaling pathway. Furthermore, DHP alleviates PDS-induced osteoporosis by increasing the expression of osteogenic markers which were decreased by the prednisolone treatment.

RUNX2 is the master transcription factor in the early stage and transdifferentiates bone marrow mesenchymal stem cells into preosteoblasts [24, 41]. OSX induces further differentiation of preosteoblasts into the mature osteoblasts and consequently promotes high expression of osteocalcin, type 1 collagen, and ALP [25, 42]. In previous, Kawane et al. found

that in *RUNX2*<sup>-/-</sup> mice, osteoprogenitors are confined to specific zones, but osteoblasts are absent, and, in *OSX*<sup>-/-</sup> mice, osteoprogenitors normally proliferates by expressing RUNX2, but an accumulation of the cells is found in the perichondrium [43]. These finding confirmed that RUNX2 is essential for the proliferation of osteoprogenitors and OSX affects osteoblasts in the late stage. In this study, we found that DHP increased expression of RUNX2, OSX, and ALP expressions both in vitro and in vivo, and upregulated vertebral formation in zebrafish larvae. Furthermore, our results revealed that DHP attenuates PDS-induced osteoporosis in zebrafish larvae by increasing the expression of *RUNX2a*, *ALP*, and *OSX* and subsequently inducing vertebral recovery. Nevertheless, many scientists revealed that combination treatment with anabolic and antiresorptive agents is more substantial and relevant therapy to cure established osteoporosis [44, 45]. Using PubMed database published in 2001-2021, Rodríguez et al. reviewed that phytochemicals such as flavonoids have a great deal of attention to osteoblastogenesis and subsequent anti-osteoporotic effects, as well as inhibition of osteoclastogenesis, though the compounds have different in their structure [46]. Furthermore, it was said their stability and safety, efficiency, degree of absorption, bioavailability, etc. must be secured before they can be applied clinically. In this, whether DHP negatively regulates osteoclastogenesis will be investigated with its safety and efficacy, which serves dual function in bone formations as an anabolic and anti-resorptive agent.

The Wnt pathway plays a central role in regulating bone formation and treatment of osteoporosis by activating  $\beta$ -catenin [20]. As known, the major two osteoblastogenic genes, including RUNX2 and OSX are regulated by a number of developmental molecules, such as Wnt/ $\beta$ -catenin and bone morphogenetic proteins [47]. Particularly, Chen and Long revealed that deletion of  $\beta$ -catenin causes severe osteopenia in OSX-lineage cells by impairing osteoblast activity and increasing osteoblast turnover [48], which indicates that  $\beta$ -catenin promotes osteoblast differentiation and activity, and indirectly suppresses osteogenesis. In this study, we

also found that DHP significantly increase GSK-3 $\beta$  phosphorylation and subsequent nuclear translocation of  $\beta$ -catenin in MC3T3E1 preosteoblasts, which may be a key regulator in DHP-induced osteoblast activation and anti-osteoporosis. Consistent with our data, in previous, many phytochemicals enhanced osteoblastogenesis via the canonical Wnt/ $\beta$ -catenin signaling pathway [20, 26, 27]. Additionally, constitutive activation of  $\beta$ -catenin inhibits osteoclast differentiation and sustains proliferation of osteoclast precursors, causing osteopetrosis [49]. Sui et al. also revealed that constitutive activation of  $\beta$ -catenin increases osteoclast numbers and consequently decreases loss of bone mass in mice [50]. Judging from the above results, more research on anti-osteoporotic effects of DHP through  $\beta$ -catenin activation is needed, because the activation of canonical Wnt/ $\beta$ -catenin signaling pathway simultaneously affects osteoblast and osteoclast, and abnormal or constitutive activation of  $\beta$ -catenin can cause bone resorption or destruction.

In conclusion, we confirmed that DHP promotes osteoblast differentiation and bone formation by activating the canonical Wnt/ $\beta$ -catenin pathway and inhibits PDS-induced osteoporosis. Taken together, we suggest that DHP may be a beneficial candidate to be used as an osteoanabolic agent.

## 5. References

1. Demontiero, O.; Vidal, C.; Duque, G., Aging and bone loss: new insights for the clinician. *Ther Adv Musculoskelet Dis* **2012**, 4, (2), 61-76.
2. Sezer, A.; Altan, L.; Ozdemir, O., Multiple Comparison of Age Groups in Bone Mineral Density under Heteroscedasticity. *Biomed Res Int* **2015**, 2015, 426847.
3. Salari, N.; Darvishi, N.; Bartina, Y.; Larti, M.; Kiaei, A.; Hemmati, M.; Shohaimi, S.; Mohammadi, M., Global prevalence of osteoporosis among the world older adults: a comprehensive systematic review and meta-analysis. *J Orthop Surg Res* **2021**, 16, (1), 669.
4. Lane, N. E., Epidemiology, etiology, and diagnosis of osteoporosis. *Am J Obstet Gynecol* **2006**, 194, (2 Suppl), S3-11.
5. Arceo-Mendoza, R. M.; Camacho, P. M., Postmenopausal Osteoporosis: Latest Guidelines. *Endocrinol Metab Clin North Am* **2021**, 50, (2), 167-178.
6. Khosla, S.; Hofbauer, L. C., Osteoporosis treatment: recent developments and ongoing challenges. *Lancet Diabetes Endocrinol* **2017**, 5, (11), 898-907.
7. Shen, C. L.; von Bergen, V.; Chyu, M. C.; Jenkins, M. R.; Mo, H.; Chen, C. H.; Kwun, I. S., Fruits and dietary phytochemicals in bone protection. *Nutr Res* **2012**, 32, (12), 897-910.
8. Buckwalter, J. A.; Cooper, R. R., Bone structure and function. *Instr Course Lect* **1987**, 36, 27-48.
9. Kim, J. M.; Lin, C.; Stavre, Z.; Greenblatt, M. B.; Shim, J. H., Osteoblast-Osteoclast Communication and Bone Homeostasis. *Cells* **2020**, 9, (9).
10. Chen, X.; Wang, Z.; Duan, N.; Zhu, G.; Schwarz, E. M.; Xie, C., Osteoblast-osteoclast interactions. *Connect Tissue Res* **2018**, 59, (2), 99-107.

11. Reid, I. R., Anti-resorptive therapies for osteoporosis. *Semin Cell Dev Biol* **2008**, 19, (5), 473-8.
12. Kim, B.; Cho, Y. J.; Lim, W., Osteoporosis therapies and their mechanisms of action (Review). *Exp Ther Med* **2021**, 22, (6), 1379.
13. Corrado, A.; Sanpaolo, E. R.; Di Bello, S.; Cantatore, F. P., Osteoblast as a target of anti-osteoporotic treatment. *Postgrad Med* **2017**, 129, (8), 858-865.
14. Miller, P. D.; Hattersley, G.; Riis, B. J.; Williams, G. C.; Lau, E.; Russo, L. A.; Alexandersen, P.; Zerbini, C. A.; Hu, M. Y.; Harris, A. G.; Fitzpatrick, L. A.; Cosman, F.; Christiansen, C.; Investigators, A. S., Effect of Abaloparatide vs Placebo on New Vertebral Fractures in Postmenopausal Women With Osteoporosis: A Randomized Clinical Trial. *JAMA* **2016**, 316, (7), 722-33.
15. Natesan, V.; Kim, S. J., Metabolic Bone Diseases and New Drug Developments. *Biomol Ther (Seoul)* **2022**, 30, (4), 309-319.
16. Vahle, J. L.; Sato, M.; Long, G. G.; Young, J. K.; Francis, P. C.; Engelhardt, J. A.; Westmore, M. S.; Linda, Y.; Nold, J. B., Skeletal changes in rats given daily subcutaneous injections of recombinant human parathyroid hormone (1-34) for 2 years and relevance to human safety. *Toxicol Pathol* **2002**, 30, (3), 312-21.
17. Pleiner-Duxneuner, J.; Zwettler, E.; Paschalis, E.; Roschger, P.; Nell-Duxneuner, V.; Klaushofer, K., Treatment of osteoporosis with parathyroid hormone and teriparatide. *Calcif Tissue Int* **2009**, 84, (3), 159-70.
18. Horcajada, M. N.; Offord, E., Naturally plant-derived compounds: role in bone anabolism. *Curr Mol Pharmacol* **2012**, 5, (2), 205-18.
19. Sharifi, S.; Moghaddam, F. A.; Abedi, A.; Maleki Dizaj, S.; Ahmadian, S.; Abdolahinia, E. D.; Khatibi, S. M. H.; Samiei, M., Phytochemicals impact on



- osteogenic differentiation of mesenchymal stem cells. *Biofactors* **2020**, 46, (6), 874-893.
20. Kim, J. H.; Liu, X.; Wang, J.; Chen, X.; Zhang, H.; Kim, S. H.; Cui, J.; Li, R.; Zhang, W.; Kong, Y.; Zhang, J.; Shui, W.; Lamplot, J.; Rogers, M. R.; Zhao, C.; Wang, N.; Rajan, P.; Tomal, J.; Statz, J.; Wu, N.; Luu, H. H.; Haydon, R. C.; He, T. C., Wnt signaling in bone formation and its therapeutic potential for bone diseases. *Ther Adv Musculoskelet Dis* **2013**, 5, (1), 13-31.
21. Mannava, A. G.; Tolwinski, N. S., Membrane bound GSK-3 activates Wnt signaling through disheveled and arrow. *PLoS One* **2015**, 10, (4), e0121879.
22. Glass, D. A., 2nd; Bialek, P.; Ahn, J. D.; Starbuck, M.; Patel, M. S.; Clevers, H.; Taketo, M. M.; Long, F.; McMahon, A. P.; Lang, R. A.; Karsenty, G., Canonical Wnt signaling in differentiated osteoblasts controls osteoclast differentiation. *Dev Cell* **2005**, 8, (5), 751-64.
23. Houschyar, K. S.; Tapking, C.; Borrelli, M. R.; Popp, D.; Duscher, D.; Maan, Z. N.; Chelliah, M. P.; Li, J.; Harati, K.; Wallner, C.; Rein, S.; Pforringer, D.; Reumuth, G.; Grieb, G.; Mouraret, S.; Dadras, M.; Wagner, J. M.; Cha, J. Y.; Siemers, F.; Lehnhardt, M.; Behr, B., Wnt Pathway in Bone Repair and Regeneration - What Do We Know So Far. *Front Cell Dev Biol* **2018**, 6, 170.
24. Ducy, P.; Zhang, R.; Geoffroy, V.; Ridall, A. L.; Karsenty, G., *Osf2/Cbfa1*: a transcriptional activator of osteoblast differentiation. *Cell* **1997**, 89, (5), 747-54.
25. Nakashima, K.; Zhou, X.; Kunkel, G.; Zhang, Z.; Deng, J. M.; Behringer, R. R.; de Crombrughe, B., The novel zinc finger-containing transcription factor *osterix* is required for osteoblast differentiation and bone formation. *Cell* **2002**, 108, (1), 17-29.
26. Karunarathne, W.; Molagoda, I. M. N.; Lee, K. T.; Choi, Y. H.; Jin, C. Y.; Kim, G. Y., Anthocyanin-enriched polyphenols from *Hibiscus syriacus* L. (Malvaceae) exert anti-

- osteoporosis effects by inhibiting GSK-3beta and subsequently activating beta-catenin. *Phytomedicine* **2021**, 91, 153721.
27. Molagoda, I. M. N.; Kang, C. H.; Lee, M. H.; Choi, Y. H.; Lee, C. M.; Lee, S.; Kim, G. Y., Fisetin promotes osteoblast differentiation and osteogenesis through GSK-3beta phosphorylation at Ser9 and consequent beta-catenin activation, inhibiting osteoporosis. *Biochem Pharmacol* **2021**, 192, 114676.
28. Molagoda, I. M. N.; Karunarathne, W.; Choi, Y. H.; Park, E. K.; Jeon, Y. J.; Lee, B. J.; Kang, C. H.; Kim, G. Y., Fermented Oyster Extract Promotes Osteoblast Differentiation by Activating the Wnt/beta-Catenin Signaling Pathway, Leading to Bone Formation. *Biomolecules* **2019**, 9, (11).
29. Foubert, K.; Dendooven, E.; Theunis, M.; Naessens, T.; Ivanova, B.; Pieters, L.; Gilissen, L.; Huygens, S.; De Borggraeve, W.; Lambert, J.; Goossens, A.; Aerts, O., The presence of benzophenone in sunscreens and cosmetics containing the organic UV filter octocrylene: A laboratory study. *Contact Dermatitis* **2021**, 85, (1), 69-77.
30. Couselo-Rodriguez, C.; Gonzalez-Esteban, P. C.; Dieguez Montes, M. P.; Florez, A., Environmental Impact of UV Filters. *Actas Dermosifiliogr* **2022**, 113, (8), 792-803.
31. Farman, S.; Javed, A.; Arshia; Khan, K. M.; Nasir, A.; Khan, A. U.; Lodhi, M. A.; Gul, H.; Khan, F.; Asad, M.; Parveen, Z., Benzophenone Sulfonamide Derivatives as Interacting Partners and Inhibitors of Human P-glycoprotein. *Anticancer Agents Med Chem* **2020**, 20, (14), 1739-1751.
32. Wu, D. L.; Liao, Z. D.; Chen, F. F.; Zhang, W.; Ren, Y. S.; Wang, C. C.; Chen, X. X.; Peng, D. Y.; Kong, L. Y., Benzophenones from *Anemarrhena asphodeloides* Bge. Exhibit Anticancer Activity in HepG2 Cells via the NF-kappaB Signaling Pathway. *Molecules* **2019**, 24, (12).

33. Chen, Y. D.; Swislocki, A. L.; Jeng, C. Y.; Juang, J. H.; Reaven, G. M., Effect of time on measurement of hepatic glucose production. *J Clin Endocrinol Metab* **1988**, 67, (5), 1084-8.
34. Arshia; Fayyaz, S.; Shaikh, M.; Khan, K. M.; Choudhary, M. I., Anti-glycemic potential of benzophenone thio/semicarbazone derivatives: synthesis, enzyme inhibition and ligand docking studies. *J Biomol Struct Dyn* **2022**, 40, (16), 7339-7350.
35. Alestrom, P.; D'Angelo, L.; Midtlyng, P. J.; Schorderet, D. F.; Schulte-Merker, S.; Sohm, F.; Warner, S., Zebrafish: Housing and husbandry recommendations. *Lab Anim* **2020**, 54, (3), 213-224.
36. Cauley, J. A., Public health impact of osteoporosis. *J Gerontol A Biol Sci Med Sci* **2013**, 68, (10), 1243-51.
37. Stern, P. H., Antiresorptive agents and osteoclast apoptosis. *J Cell Biochem* **2007**, 101, (5), 1087-96.
38. Zhang, J.; Saag, K. G.; Curtis, J. R., Long-term safety concerns of antiresorptive therapy. *Rheum Dis Clin North Am* **2011**, 37, (3), 387-400, vi.
39. Weinstein, R. S., Glucocorticoid-induced osteoporosis and osteonecrosis. *Endocrinol Metab Clin North Am* **2012**, 41, (3), 595-611.
40. Haas, A. V.; LeBoff, M. S., Osteoanabolic Agents for Osteoporosis. *J Endocr Soc* **2018**, 2, (8), 922-932.
41. Komori, T., Regulation of Proliferation, Differentiation and Functions of Osteoblasts by Runx2. *Int J Mol Sci* **2019**, 20, (7).
42. Liu, Q.; Li, M.; Wang, S.; Xiao, Z.; Xiong, Y.; Wang, G., Recent Advances of Osterix Transcription Factor in Osteoblast Differentiation and Bone Formation. *Front Cell Dev Biol* **2020**, 8, 601224.

43. Kawane, T.; Qin, X.; Jiang, Q.; Miyazaki, T.; Komori, H.; Yoshida, C. A.; Matsuura-Kawata, V.; Sakane, C.; Matsuo, Y.; Nagai, K.; Maeno, T.; Date, Y.; Nishimura, R.; Komori, T., Runx2 is required for the proliferation of osteoblast progenitors and induces proliferation by regulating Fgfr2 and Fgfr3. *Sci Rep* **2018**, 8, (1), 13551.
44. Cosman, F., Anabolic and antiresorptive therapy for osteoporosis: combination and sequential approaches. *Curr Osteoporos Rep* **2014**, 12, (4), 385-95.
45. Leder, B. Z., Optimizing Sequential and Combined Anabolic and Antiresorptive Osteoporosis Therapy. *JBMR Plus* **2018**, 2, (2), 62-68.
46. Rodriguez, V.; Rivoira, M.; Picotto, G.; de Barboza, G. D.; Collin, A.; Tolosa de Talamoni, N., Analysis of the Molecular Mechanisms by Flavonoids with Potential Use for Osteoporosis Prevention or Therapy. *Curr Med Chem* **2022**, 29, (16), 2913-2936.
47. Zhang, H.; Recker, R.; Lee, W. N.; Xiao, G. G., Proteomics in bone research. *Expert Rev Proteomics* **2010**, 7, (1), 103-11.
48. Chen, J.; Long, F., beta-catenin promotes bone formation and suppresses bone resorption in postnatal growing mice. *J Bone Miner Res* **2013**, 28, (5), 1160-9.
49. Wei, W.; Zeve, D.; Suh, J. M.; Wang, X.; Du, Y.; Zerwekh, J. E.; Dechow, P. C.; Graff, J. M.; Wan, Y., Biphasic and dosage-dependent regulation of osteoclastogenesis by beta-catenin. *Mol Cell Biol* **2011**, 31, (23), 4706-19.
50. Sui, X.; Deng, S.; Liu, M.; Fan, L.; Wang, Y.; Xu, H.; Sun, Y.; Kishen, A.; Zhang, Q., Constitutive Activation of beta-Catenin in Differentiated Osteoclasts Induces Bone Loss in Mice. *Cell Physiol Biochem* **2018**, 48, (5), 2091-2102.

